

Fast Analysis of a Compound Large Reflector Antenna

by

Stéphanie Alphonse

Thesis presented in partial fulfilment of the requirements for
the degree of Master of Science in Engineering at
the University of Stellenbosch



Department of Electrical and Electronic Engineering,
University of Stellenbosch

Supervisors:
Prof K.D. Palmer and Dr D.I.L de Villiers

March 2012

Declaration

By submitting this thesis electronically, I declare that the entirety of the work contained therein is my own, original work, that I am the sole author thereof (save to the extent explicitly otherwise stated), that reproduction and publication thereof by Stellenbosch University will not infringe any third party rights and that I have not previously in its entirety or in part submitted it for obtaining any qualification.

Date: March 2012

Abstract

The offset Gregorian dual reflector antenna is eminently well suited to a radio telescope antenna application as it offers a narrow beam width pattern (i.e high gain) and good efficiency. The focus of this work is on the analysis of characteristics of such a Gregorian antenna.

The design of the class of reflector antennas is normally based on the use of ray-optics, with this simplified approach being able to predict antenna performance based on approximate formulas for example the beam width against aperture size. However for compound antennas such as the Gregorian reflector there are several interdependent parameters that can be varied and this reduces the applicability of the simple ray-optic approach. It was decided that, if a fast enough analysis of a configuration can be found, the technique of design through interactive analysis would be viable.

To implement a fast analysis of the main beam performance of such a Gregorian antenna, a solution algorithm has been implemented using a plane wave spectrum approach combined with a custom aperture integration formulation. As this is able to predict the beam performance within about a second on a PC, it is suitable for iterative design. To implement the iterative design in a practical manner a user interface has been generated that allows the user to interactively modify the geometry, see the physical layout, and then find the antenna pattern. A complete working system has been realised with results comparing well to a reference solution. The limitations of the technique, such as its inaccuracy in predicting the side lobe structure, are also discussed.

Opsomming

Die afset Gregoriaanse dubbelweerkatser antenna is uiters gepas vir radioteleskoop toepassings aangesien dit 'n nou bundelwydte (hoë aanwins) en 'n goeie benuttingsgraad bied. Die fokus van hierdie werk is op die analise van die eienskappe van so 'n Gregoriaanse antenna.

Die ontwerp van die klas van weerkaatsantennas is normaalweg gebaseer op straal-optika, waar hierdie vereenvoudigde tegniek, deur benaderde formules, gebruik kan word om antennawerkverrigting af te skat soos bv. die bundelwydte teen stralingsvlakgrootte. Vir saamgestelde antennes soos die Gregoriaanse weerkatser is daar egter verskeie onafhanklike parameters wat verstel kan word en die toepaslikheid van die eenvoudige straal-optiese benadering verminder. Dit was besluit dat, indien die analise van die konfigurasie vinnig genoeg uitgevoer kon word, die tegniek van ontwerp deur interaktiewe analise werkbaar kan wees.

Om 'n vinnige analise van die hoofbundelwerkverrigting van so 'n Gregoriaanse antenna te bewerkstellig, is 'n oplossingsalgoritme gementeer wat gebruik maak van 'n platvlakgolfspektrum benadering in kombinasie met 'n doelgemaakte stralingsvlakintegrasieformulering. Aangesien hierdie strategie die hoofbundel binne ongeveer 'n sekonde op 'n persoonlike rekenaar kan voorspel, is dit gepas vir iteratiewe ontwerp. Om die iteratiewe ontwerp op 'n praktiese wyse te implementeer is 'n gebruikerskoppelvlak geskep wat die gebruiker toelaat om, op 'n interaktiewe wyse, die geometrie aan te pas, die fisiese uitleg te sien en dan die stralingspatroon te bereken. 'n Volledige werkende stelsel is gerealiseer met resultate wat goed ooreenstem met 'n verwysingsoplossing. Die tekortkominge van die tegniek, soos die onakkuraatheid in die voorspelling van die sylobstruktuur, word ook bespreek.

Acknowledgements

I would like to express my gratitude to the following people and organisations for their contribution towards this project:

- My academic supervisors Prof. Keith D. Palmer and Dr Dirk I.L. de Villiers for their comprehensive and invaluable guidance in completing this work.
- Prof. Howard Reader for his confidence in me and the suggestion to attend various electromagnetic courses.
- Prof. Gerard Rambolamanana for his guidance and advice to adjust my watch to be on time.
- Hasimboahangy Samuël R. for her love and patience.
- Anita van der Spuy for her proofreading of this report.
- EMSS for the use of FEKO software which they made available for simulation purposes.
- The South African SKA project for the financial support during my Masters.
- Last but not the least to my family in Madagascar for their love, support and encouragements during the last two and half years.

”In the middle of difficulty lies opportunity” Albert Einstein.

*To my nephews: Joe-Georgio A., Jean-Yves Alphonse A.
and nieces: Erwine Trishilla A., Marie-Joanna A.*

Contents

Declaration	i
Abstract	ii
Opsomming	iii
Acknowledgements	iv
Table of contents	vi
List of figures	ix
List of tables	xi
Nomenclature	xiii
1 Introduction	1
1.1 Background to the Project	1
1.2 Objectives and Outline of this Thesis	2
2 General Theory of Reflector Antennas	3
2.1 Types of reflector antennas	4
2.1.1 Single reflector	4
2.1.2 Dual reflector	5
2.2 Directivity and Gain:	6
2.2.1 Principles of a paraboloid reflector	7
2.2.2 Directivity:	8
2.2.3 Gain of the reflector antenna:	9
2.3 Aperture efficiency η_{ap} :	9
2.3.1 Illumination efficiency η_t :	11
2.3.2 The spillover efficiency η_s :	12
2.3.3 The polarization efficiency η_{pol} :	13

2.3.4	The phase efficiency η_ϕ :	13
2.3.5	The surface error efficiency η_r :	14
2.4	Summary	14
3	High-frequency Methods for Reflector Antennas	15
3.1	Radiation structures	15
3.1.1	Radiation current source	16
3.1.2	Aperture distribution source	18
3.2	Geometric Optics theory	20
3.2.1	Propagation of rays in Geometrical Optics	21
3.2.2	Reflection on the boundary	22
3.2.3	Propagation power of the rays	23
3.3	Physical Optics theory	23
3.3.1	Induced current density for PEC	24
3.3.2	PO radiation fields	24
3.3.3	Dual-reflector application	25
3.4	Analysis of the diffraction effect on the sub-reflector rim	26
3.4.1	Huygens-Fresnel principle of diffraction	26
3.4.1.1	Edge diffraction in the sub-reflector surface	27
3.4.2	Geometrical Theory of Diffraction	28
3.4.2.1	Geometrical Optics fields	28
3.4.2.2	Diffracted fields on a curved surface	28
3.4.3	Physical Theory of Diffraction	31
3.4.3.1	Method of Equivalent Current	32
3.5	Antenna Radiation pattern using Plane Wave Spectrum	32
3.5.1	Plane waves spectrum representation	33
3.5.2	The Angular spectrum approximation	34
3.6	Conclusion	35
4	Description of a Gregorian Reflector Antenna and Creation of a FEKO Reference	36
4.1	Description of the Gregorian Reflector Antenna	37
4.1.1	Gregorian geometry structure	37
4.1.2	Main Reflector	38
4.1.2.1	Characteristics of the Main Reflector	38
4.1.2.2	Main reflector parameters	38
4.1.3	Sub-reflector	39
4.1.3.1	Characteristics of the sub-reflector	39

Contents

4.1.3.2	Reflection from the sub-reflector	40
4.1.4	Equivalent parabola analysis	41
4.1.5	Antenna design parameters	42
4.1.5.1	Ellipsoid parameters	42
4.1.5.2	Paraboloid design parameters	44
4.2	Creation of a Gregorian antenna Reference in FEKO	45
4.2.1	The system feed	45
4.2.1.1	Simulation in FEKO	45
4.2.1.2	Method Of Moments	46
4.2.1.3	Results gain of the feed	46
4.2.1.4	Advantages of using a dual reflector	47
4.2.2	Gregorian reflector antenna simulation using hybrid technique	48
4.2.2.1	FEKO simulation set-up	49
4.2.2.2	Feed pattern description	49
4.2.2.3	Sub-reflector pattern	50
4.2.2.4	Radiation pattern of the Gregorian antenna system	51
4.3	Conclusion	53
5	Fast Approximation Technique for Reflector Antenna Patterns	54
5.1	Radiation pattern of the sub-reflector using PWS	55
5.2	Radiation of the main reflector	59
5.2.1	Aperture Integral Technique	59
5.2.2	Gauss Legendre technique	60
5.3	Comparison of the fast approximation results with FEKO	62
5.4	Matlab GUI application	66
5.4.1	Overview of the GUI	66
5.4.2	GUI design	67
5.4.2.1	Input parameters	67
5.4.2.2	Computation of results	67
5.4.2.3	Plots of the Geometry and Pattern	68
5.5	Conclusion	68
6	Conclusions	69
	Bibliography	70
A	Analytical evaluation of directivity using spectrum [1].	A-1
A.1	Directivity using PWS	A-1
A.2	The total radiated power	A-2

List of Figures

1.1	Prototype of a dual offset Gregorian dual reflector antenna for MeerKAT . . .	2
2.1	Types of reflector antenna	4
2.2	Paraboloid single reflector antenna	5
2.3	Geometry of two types of dual reflector antenna	6
2.4	Geometry of parabolic reflector	7
2.5	Aperture efficiency for different feed patterns as function of θ_0	11
2.6	Taper or illumination efficiency for different feed patterns as function of θ_0 .	11
2.7	Spillover efficiency for different feed patterns	12
2.8	Trade-off between spillover and taper efficiencies	13
3.1	Distribution of currents on a reflector surface	17
3.2	Radiation fields on a reflector aperture plane	19
3.3	Primary and secondary wave of radiated wave	21
3.4	Derivation from Snell's Law	22
3.5	Offset Gregorian dual reflector coordinate	25
3.6	Huygens construction	26
3.7	Rays diffracted in the parabolic reflector edges	27
3.8	Diffracted rays at a curved edge	29
3.9	Coordinate system of the plane wave propagation	33
4.1	Front and side view of a Gregorian dual reflector	37
4.2	Ellipsoid geometry	40
4.3	Equivalent paraboloid of a dual offset Gregorian geometry with circular aperture	41
4.4	An offset Gregorian dual reflector antenna geometry	45
4.5	Ideal source oriented towards a paraboloid reflector with the diameter of the dish $D = 50\lambda$, generated with <i>FEKO</i>	46
4.6	Comparison of approximate gain from the full-wave results from FEKO and the analytical approximation for different sources	47
4.7	Model in 3D of an Offset Gregorian Dual reflector	48

List of Figures

4.8	Idealised feed pattern	50
4.9	3D geometry of the sub-reflector	50
4.10	Radiation pattern of a 16.67λ sub-reflector for different frequencies	51
4.11	3D geometry of the paraboloid of the dish	52
4.12	Radiation pattern of an offset Gregorian dual reflector antenna in H and E-plane for $f/D=0.3333$	52
4.13	Radiation pattern of an offset Gregorian dual reflector antenna in H and E-plane for $f/D=0.65$	53
5.1	Rectangular mesh grid of the cut surface of the ellipsoid sub-reflector	56
5.2	Front and side view of the aperture E-field on the sub-reflector	57
5.3	Cut-off field on the sub-reflector aperture	57
5.4	Diffraction term on the sub-reflector aperture	58
5.5	Diffraction term back transformed at the origin	58
5.6	Top and side view of the sub-reflector cut radiation pattern	59
5.7	Orientation of the new source towards the Main reflector	60
5.8	Radiation pattern of the reflector for 1 GHz frequency using PWS approach	61
5.9	Radiation pattern of the reflector for 1.25 GHz frequency using PWS approach	62
5.10	Radiation pattern of the reflector for 2 GHz frequency using PWS approach	62
5.11	Comparison of the fast approximation technique and the numerical simulation of the dual reflector radiation pattern in E- and H-plane at $\text{freq}= 1 \text{ GHz}$. .	63
5.12	Comparison of the fast approximation technique and the numerical simulation of the dual reflector radiation pattern in E- and H-plane at $\text{freq}= 1.25 \text{ GHz}$.	64
5.13	Comparison of the fast approximation technique and the numerical simulation of the dual reflector radiation pattern in E- and H-plane at $\text{freq}= 2 \text{ GHz}$. .	65
5.14	A quick visualisation of Gregorian dual reflector properties	67

List of Tables

4.1	Gregorian design parameters	38
4.2	Parameter Values computed from the design equations	44
4.3	Parameters of the antenna design	49
5.1	Comparison of the beamwidth results	66

Nomenclature

List of abbreviations

2D	Two dimensional
CAD	Computer-aided Design
CEM	Computational Electromagnetic
GO	Geometrical Optics
GTD	Geometrical Theory of Diffraction
GUI	Graphical User Interface
HF	High frequency
HPBW	Half Plane Beam Width
MEC	Method of Equivalent Current
MeerKAT	Karoo Array Telescope
MLFMM	Multilevel Fast Multipole Method
MoM	Method of Moments
PEC	Perfect Electric Conductor
PO	Physical Optics
PTD	Physical Theory of Diffraction
PWS	Plane Wave Spectrum
rms	Root Mean Square
SKA	Square Kilometre Array
SLL	Side Lobe Level
uicontrol	User Interface Control
uimenu	User Interface Menu
VSWR	Voltage Signal Noise Ratio

Constants and Units

ϵ, ϵ_0	General and free space permittivity	F/m
η	intrinsic impedance of free space ($\eta = \sqrt{\frac{\mu_0}{\epsilon_0}}$)	Ω

Nomenclature

λ	wavelength	m
μ, μ_0	General and free space permeability	H/m
k_0	wave number in free space	rad.s ⁻¹
ω	angular frequency	rad/s ⁻¹

Symbols and Units

\bar{A}	Electric vector potential	Wb/m
\bar{A}_m	Magnetic vector potential	W/m ²
\bar{B}	Magnetic flux density	Wb/m ²
\bar{D}	Electric flux density	C/m ²
\bar{E}	Electric field intensity (spatial form)	V/m
\bar{H}	Magnetic field intensity (spatial form)	A/m
\bar{J}, \bar{J}_m	Electric and magnetic currents	A
$\bar{J}_{es}, \bar{J}_{ms}$	Electric and magnetic current densities	A/m ²
\bar{S}	Time average Poynting vector	V

Chapter 1

Introduction

1.1 Background to the Project

IT is hoped that the innovation of designing a powerful radio telescope, which will operate over a wide microwave frequency range, scan and map the sky with 50-100 times more sensitivity than any present-day radio telescope, has been entrusted to the South Africa Square Kilometre Array(SKA SA) project [2]. This large telescope is intended to solve various problems experienced by astronomers, cosmologists and other scientists and to determine the nature of dark matter or dark energy [3].

The MeerKAT project, which is a precursor of the SKA, is adopting a new antenna geometry to increase the efficiency of the reflectors. This new design, the offset Gregorian dual reflector antenna, illustrated in Figure 1.1, is a solution to feed blockage limitations of the preceding telescope. The MeerKAT will install an array of 64 of these antennas in South African site, each of them having a primary reflector with a diameter of 13.5m and a smaller concave secondary reflector. This antenna geometry with its clear optical path and low side lobe level results, will probably be the geometry adopted for the SKA [4]. Most commercial software package tools cannot analyse such large antennas efficiently due to the excessive computational time and memory storage constraints. Finding a fast approximate solution is thus the focus of the work.



Figure 1.1: Prototype of a dual offset Gregorian dual reflector antenna for MeerKAT [3]

1.2 Objectives and Outline of this Thesis

The offset dual reflector antennas are very popular because they offer good pattern performance with low side lobes and high efficiency. As these are best suited to high gain antennas, they are electrically large and their design can be based on ray-optics where all secondary effects such as diffraction are ignored. The main objective of this thesis is to devise a scheme that will allow for iterative design of an offset Gregorian reflector antenna. For that, a fast quasi-analytical technique will be presented that will be shown to predict main beam performance well. This technique allows the user to evaluate the design quickly enough on a PC and develops an understanding of effect of the geometrical parameters on the antenna performance.

A number of a sub-objectives are set to reach this objective:

1. Chapter 2 gives a brief introduction of reflector antennas
2. Some of the high frequency techniques that can be used with such a large antenna to speed up the solution are discussed in Chapter 3
3. Section 4.1 introduces the description and design parameters of an offset Gregorian dual reflector antenna;
4. Section 4.2 discusses the creation of a reference solution for a specific geometry using the FEKO commercial software, so as to have a solution to which approximate solution can be compared.
5. Chapter 5 describes an implementation of a suitable fast method of finding a Gregorian radiation pattern and its full solution.

All numerical computation and results are obtained using DELL computer, equipped with a dual core processor working at 3 GHz and with 4GB of RAM.

Chapter 2

General Theory of Reflector Antennas

Introduction

AN antenna is a transducer device that converts a guided electromagnetic wave on a transmission line into a plane wave radiating in free space[5]. Various types of antennas are used in radar or satellite communication. The most widely used for narrow beam antenna are reflector antennas.

These antennas are composed basically of a primary feed and one or several reflectors where the reflectors shape or deflect the radiation from the primary feed source which may typically be a horn, dipole or microstrip antenna. Horns are commonly used for radio telescopes because they provide a suitable symmetrical pattern, high efficiency, low VSWR (with waveguide feeds) and relatively wide bandwidth. Diverse geometrical configurations of reflector antennas can be seen in practice but the conventional reflector designs are planar, corner or curved reflector, as depicted in Figure 2.1. The radiation pattern of the antenna system is affected by several parameters such as the radiation pattern of the feed, the shape and the size of the reflectors which can give rise to spillover, diffraction and the aperture blockage effect.

This chapter highlights the paraboloid reflector geometry. Types of reflector antennas are described in section 2.1 and the parameters of the antenna are investigated in section 2.2 and 2.3 respectively.

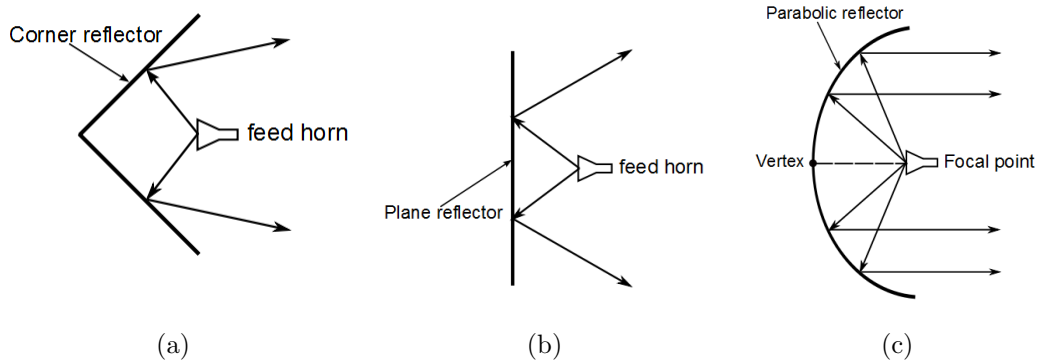


Figure 2.1: Geometry of (a) aperture distribution corner reflector, (b) plane reflector and (c) parabolic curved reflector after [6]

2.1 Types of reflector antennas

Reflector antennas are pencil beam antennas that may have one or more reflectors with the larger reflector often shaped with a paraboloid. The paraboloid transforms a spherical wave radiated by the feed located at the antenna focal point into a plane wave. Because of this geometrical property, paraboloidal reflector antennas find application where a high gain is desired, typically 30-40 dB, along with low cross polarization [7].

The number of reflectors used depends upon the application and also on the extent to which it is necessary to optimise the efficiency of the antennas. Both dual and single reflectors find application in radar and satellite communication. The next section will discuss the characteristics and application of single and dual reflector antennas.

2.1.1 Single reflector

A single reflector antenna consists of a primary feed and a reflector facing it. The single reflector antenna can be symmetrically fed from the reflector focal point or offset fed, as illustrated on 2.2. Reflector surfaces are based on the conic sections: paraboloid, hyperboloid or ellipsoid. Paraboloid reflectors are the simplest for narrow beamwidth, while ellipsoidal and hyperboloidal sub-reflectors are usually applied to relocate focal points in quasi-optical systems.

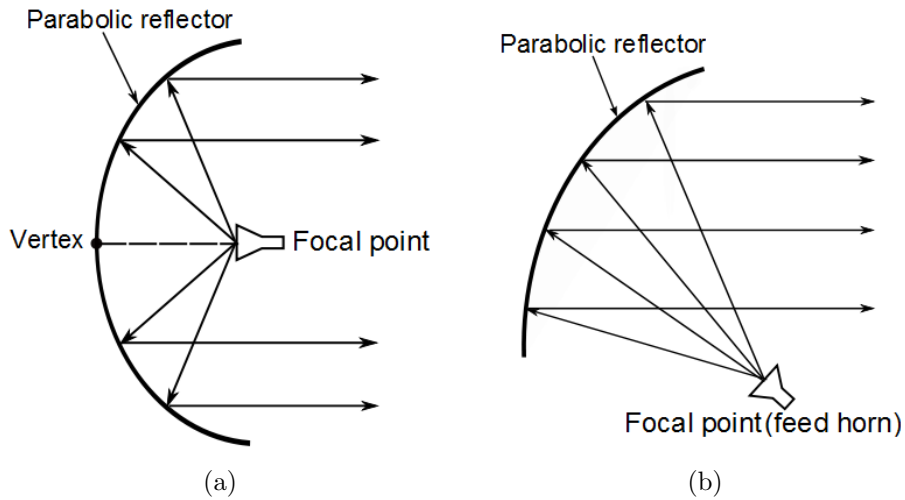


Figure 2.2: (a) Front and, (b) offset fed paraboloid reflector antenna

Besides possible mechanical issues, the disadvantage of using a single reflector is the feed blockage effects. This blockage reduces the aperture efficiency and thus antenna gain as well as influencing the side lobe level negatively. In addition, scattering from the feed support structure and struts also degrade pattern performance as do possible multiple reflections between the feed and the reflector.

2.1.2 Dual reflector

Dual reflector antennas are popular in low noise earth terminal applications. They include a second reflector, placed between the feed and the prime reflector of a single reflector antenna. This second reflector so called *sub-reflector*, usually smaller than the main reflector overcomes many of the disadvantages of the single reflector.

The basic dual paraboloid reflector antennas are derived from an optical telescope invented in the 17th century by James Gregory and Laurent Cassegrain. The Gregorian antenna has an ellipsoidal sub-reflector, which decreases the effective focal length of the system. Cassegrain antennas use an hyperboloidal sub-reflector to increase the effective focal length. The geometry of both antenna types is shown in Figure 2.3. The variation in the effective focal length directly affects the antenna gain and the side lobe level. Increasing this parameter for example, will higher the side lobe level and the spillover [8].

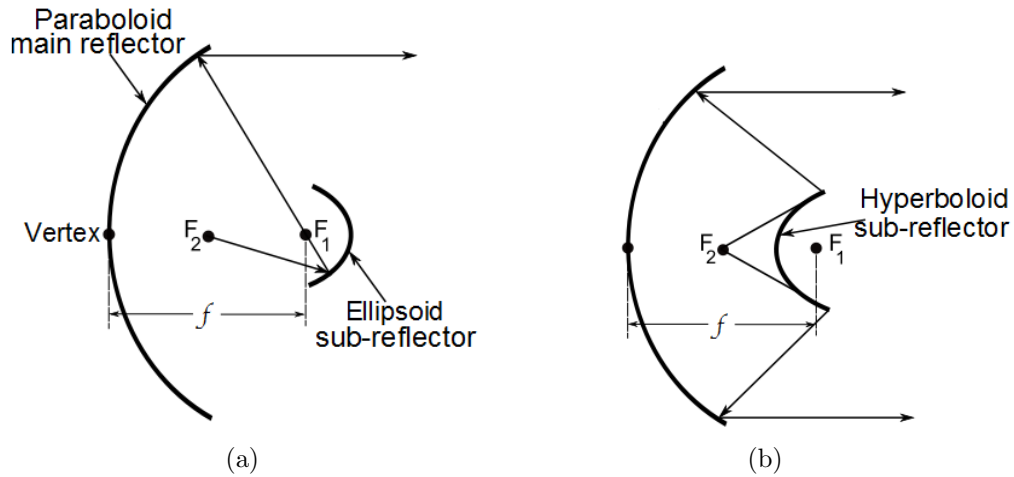


Figure 2.3: Geometry of (a) Gregorian and (b) Cassegrain reflector antenna

F_1 and F_2 are the focus points of the sub-reflector and the main reflector, and f is the focal length of the main reflector. F_1 is a virtual point from which transmitted rays appear to emanate with a spherical wave front after being reflected from the sub-reflector. This sub-reflector causes the antenna feed to be directed towards the apex of the main reflector, which removes the feed from the active aperture. When designing a reflector antenna the directivity, gain and the aperture efficiency are the most important parameters to be considered.

2.2 Directivity and Gain:

The reflector is usually a metallic surface formed into a paraboloid of revolution and truncated by a circular rim that forms the diameter of the antenna. Figure 2.4 depicts the basic geometry of a paraboloid reflector antenna.

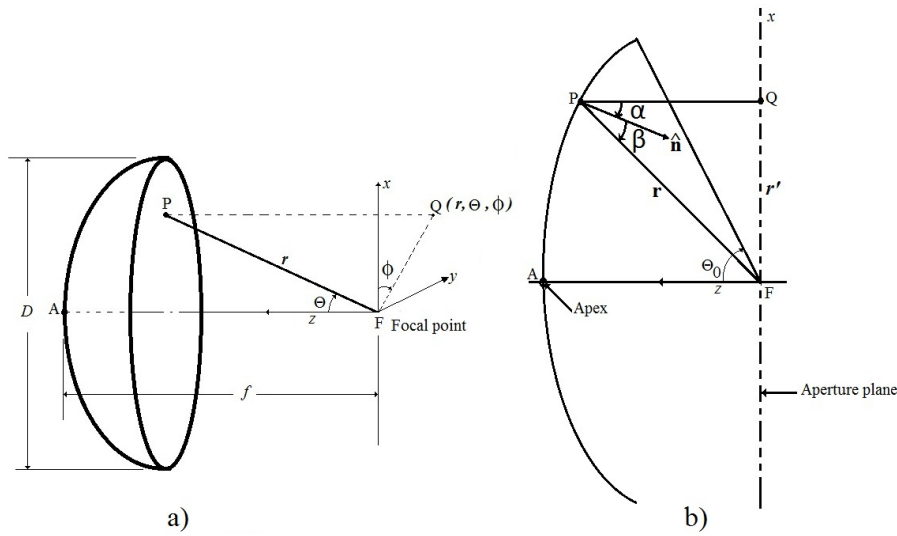


Figure 2.4: Geometry of parabolic reflector: a) coordinate system, b) cross section of the aperture plane [8].

A reflector antenna system has several significant parameters, and associated terms such as:

1. focus(or focal point): is the point relative to the parabolic reflector at which any incoming signals are concentrated after the reflector. The source of the radiation of the parabola is placed at this point to illuminate the parabolic reflector.
2. Vertex: it is innermost point at the centre of the parabolic reflector,
3. The ratio f/D : defines the axis symmetric paraboloidal reflector. As the f/D ratio is often specified along with the diameter D , the focal length f can be obtained very easily by multiplying its f/D ratio by the specified diameter.
4. Aperture: it is the surface, near or on the antenna, on which it is convenient to make assumption regarding the field values for the purpose of computing a field at external points [9].

2.2.1 Principles of a paraboloid reflector

The surface of a paraboloidal reflector is made by rotating a parabola about its axis. From Figure 2.4, the distance from the focal point F into the surface point of the paraboloid is:

$$FP = r \quad (2.2.1)$$

The projection of this point P into the aperture plane is Q , and the distance through the focal point is $FQ = r \cos \theta$. In a parabola the distance from the source, the focal point, to

the point Q via the reflector is the same for all points Q.

$$FP + FQ = 2f \quad (2.2.2)$$

By replacing the FP and PQ by their values, then (2.2.2) becomes:

$$r + r\cos\theta = 2f \quad (2.2.3)$$

or

$$r = \frac{2f}{1 + \cos\theta} = f \sec^2\left(\frac{\theta}{2}\right) \text{ with } \theta \leq \theta_0 \quad (2.2.4)$$

Equation (2.2.4) defines the paraboloid equation in spherical coordinates (r, θ, ϕ) , and only a function of the angle θ because of the rotational symmetry. It can also be expressed in rectangular coordinates:

$$r'^2 = 4f(f - z) \text{ with } r' \leq Q \quad (2.2.5)$$

Another important parameter on the paraboloid is the reflector angle called *the subtended angle of the reflector* θ_0 .

$$\tan(\theta_0) = \frac{\left(\frac{D}{2}\right)}{z} \quad (2.2.6)$$

where z is the distance on the z axis from the focal point into the edge of the paraboloid reflector and D is the diameter of the dish. This angle can also be expressed in another form f/D . It describes the curvature of the paraboloid and typically ranges from 0.3 to 1 [8].

$$f = \frac{D}{4} \cot\left(\frac{\theta_0}{2}\right) \quad (2.2.7)$$

2.2.2 Directivity:

Directivity is the ratio of the radiation intensity in the (θ, ϕ) direction to the average radiation intensity over all directions. The average radiation intensity is equal to the total power radiated divided by 4π [10].

The focal length f determines how the power from the feed is spread over the aperture plane. If $G_f(\theta, \phi)$ is the feed pattern, which is assumed to be circularly symmetric to simplify the analysis, it has no component on the ϕ angle. The directivity of the reflector antenna can be written as:

$$D = \frac{U(\theta, \phi)}{U(\theta, \phi)_{av}} = \frac{4\pi U(\theta = \pi)}{P_t} \quad (2.2.8)$$

where P_t is the total radiated power in [W] and U is the radiation intensity in [W/unit solid

angle]. It can also be expressed in terms of the feed pattern as [6]:

$$D = \frac{16\pi^2}{\lambda^2} f^2 \left| \int_0^{\theta_0} \sqrt{G_f(\theta)} \tan\left(\frac{\theta}{2}\right) d\theta \right|^2 \quad (2.2.9)$$

where λ is the wavelength.

2.2.3 Gain of the reflector antenna:

It is difficult to find the total power radiated by the antenna in practice; however, a parameter of interest is the ability of the antenna to transform the available power at its input terminal to the radiated power. This quantity is defined as the gain of the antenna. It is the ratio of the radiation intensity in a given direction from the antenna to the total input power accepted by the antenna per unit solid angle.

$$G(\theta, \phi) = \frac{4\pi U(\theta = \pi)}{P_{in}} \quad (2.2.10)$$

where $U(\theta = \pi)$ expresses the radiation intensity only on θ angle, because of the symmetrical axis, and P_{in} is the input power radiated by the antenna.

The relationship between the power gain and the directivity of an antenna can be given by comparing (2.2.8) and (2.2.10):

$$G(\theta, \phi) = \frac{P_t}{P_{in}} D(\theta, \phi) = \eta_{rad} D(\theta, \phi) \quad (2.2.11)$$

η_{rad} is the radiated efficiency of the antenna, the ratio of the total radiation power to the input power radiated by the antenna. This factor is generally greater than 0 and less than 1 ($0 \leq \eta_{rad} \leq 1$). The radiation efficiency of the reflector antennas refers to ohmic losses because the parabolic reflector is typically metallic, with a high conductivity. Another efficiency factor, which relates the directivity of the system to that an uniform aperture at same size is the aperture efficiency. Details of this factor will be discussed in the subsequent section.

2.3 Aperture efficiency η_{ap} :

The aperture efficiency can be decomposed into sub-efficiencies composed of the illumination efficiency η_t , the spillover efficiency η_s , the phase efficiency η_ϕ , the polarization efficiency η_{pol} and the surface error efficiency η_r [11]. Thus, the total aperture efficiency is the product

of these factors which can be written as:

$$\eta_{ap} = \eta_t \eta_s \eta_\phi \eta_{pol} \eta_r \quad (2.3.1)$$

η_{ap} varies with the position and the pattern of the feed. A class of the radiation pattern is defined by Silver in literature as [12]:

$$G_f(\theta) = \begin{cases} G_0^{(n)} \cos^n(\theta) & 0 \leq \theta \leq \frac{\pi}{2} \\ 0 & \frac{\pi}{2} \leq \theta \leq \pi \end{cases} \quad (2.3.2)$$

where n is a positive integer ($n \geq 1$), $G_0^{(n)}$ is a constant for a given n and is determined from the relation [6]:

$$\iint_S G_f(\theta) d\Omega = \iint_S G_f(\theta) d\theta d\phi = 4\pi \quad (2.3.3)$$

From this the constant $G_0^{(n)}$ can be computed:

$$\int_0^{\pi/2} G_0^{(n)} \cos^n(\theta) \sin\theta d\theta = 2 \quad (2.3.4)$$

where

$$G_0^{(n)} = 2(n+1) \quad (2.3.5)$$

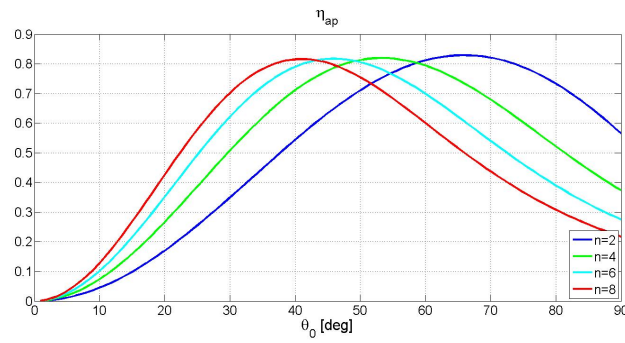
and hence, the feed pattern in (2.3.2) becomes:

$$G_f(\theta) = \begin{cases} 2(n+1) \cos^n(\theta) & 0 \leq \theta \leq \frac{\pi}{2} \\ 0 & \frac{\pi}{2} \leq \theta \leq \pi \end{cases} \quad (2.3.6)$$

The aperture efficiency is expressed in terms of the radiation feed pattern of the antenna as [6]:

$$\eta_{ap} = \cot\left(\frac{\theta}{2}\right)^2 \left| \int_0^{\theta_0} \sqrt{G_f(\theta \tan\left(\frac{\theta}{2}\right))} d\theta \right|^2 \quad (2.3.7)$$

θ_0 is the half-angle of the reflector for a single reflector. An example calculation of aperture efficiency for a paraboloid reflector design is shown in Figure 2.5. The result shows that for each θ_0 , which is a function of f/D ratio, there is a value for n that maximizes the aperture efficiency. The diameter D is of primary concern for the design. Clearly it should be made as large as possible so that the physical aperture is maximized, but as it is one of the primary cost drivers where compromise must be made.


 Figure 2.5: Aperture efficiency for different feed patterns as function of θ_0

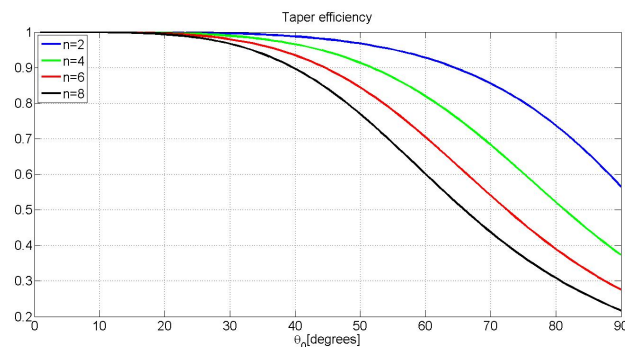
2.3.1 Illumination efficiency η_t :

The illumination efficiency or "*taper efficiency*" is a measure of the non uniformity of the field across the aperture caused by the tapered radiation pattern.

For a reflector antenna, the geometric area must be greater than the effective area because the illumination is less towards the edges. In terms of the feed pattern, it can be computed by the ratio of the maximum radiation intensity integrated over all the aperture and the power intercepted by the aperture.

$$\eta_t = \frac{U_{max}}{P_{int}} = 2 \cot\left(\frac{\theta_0}{2}\right)^2 \frac{\left| \int_0^{\theta_0} \sqrt{G_f(\theta)} \tan\left(\frac{\theta}{2}\right) d\theta \right|^2}{\int_0^{\theta_0} G_f(\theta_f) \sin\theta d\theta} \quad (2.3.8)$$

This efficiency can be increased with the f/D ratio. Figure 2.6 depicts the variation of the taper efficiency with the subtended angle θ_0 of the reflector.


 Figure 2.6: Taper or illumination efficiency for different feed patterns as function of θ_0

2.3.2 The spillover efficiency η_s :

Spillover efficiency is defined as the proportion of energy from the feed source that is intercepted by the reflector (see Figure 2.3.2). Considering that the feed is sitting on a symmetrical axis, then the spillover is:

$$\eta_s = \frac{P_{int}}{P_{rad}} = \frac{\int_0^{\theta_0} G_f(\theta) \sin\theta d\theta}{\int_0^{\pi} G_f(\theta) \sin\theta d\theta} \quad (2.3.9)$$

In practice this efficiency can be improved by moving the feed closer to the reflector, or by increasing its diameter D .

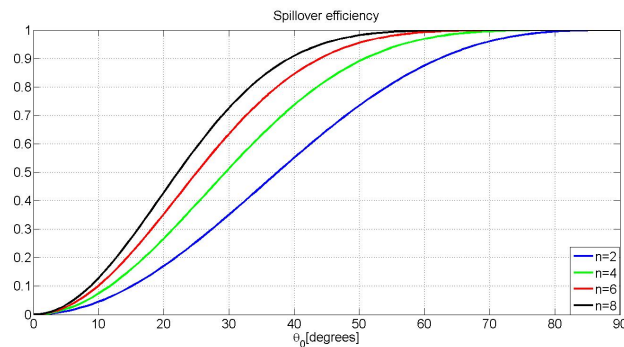


Figure 2.7: Spillover efficiency for different feed patterns

These two sub-efficiencies, spillover and taper, are cross-complementary. The spillover efficiency will increase with the edge taper, which is the ratio of the field at the edge to the field at the centre of the reflector, while the illumination efficiency decreases. The compromise between the two efficiencies can be used to find an optimum solution, as shown in Figure 2.8,

where they are given as a function of the subtended angle θ_0 for different values of n for the radiation feed pattern. In practice this trade-off generates a maximum value of $\eta_t \eta_s$ with an edge taper of about -11 dB [8].

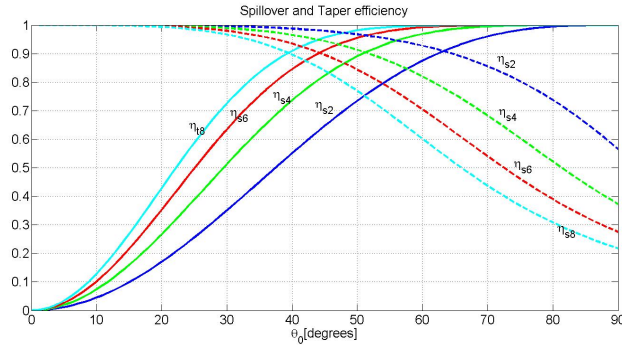


Figure 2.8: Trade-off between spillover and taper efficiencies

2.3.3 The polarization efficiency η_{pol} :

Polarization of an antenna is defined as the position and the direction of the electric field with reference typically to the ground or surface of the earth. Depending on the orientation of the electric and the magnetic fields, the polarization can be classified as linear, circular or elliptical. Linear and circular polarization are special cases of elliptical polarization, when the ellipse becomes a straight line or circle, respectively. For linear polarization, if the field is oriented parallel to the ground, the polarization is called horizontal and the polarization is known as vertical when the electric field is perpendicular to the ground. For the circular case, the clockwise rotation of the electric field vector is designated as right-handed polarization (RH) and left-handed polarization (LH) is the counter-clockwise, for an observer looking in the direction of propagation [13],[14].

The polarization efficiency is the ratio of the power in the desired polarization P_{co} to the total power intercepted by the reflector. It is affected by the polarization losses and can be computed through the co and cross-polarization radiation patterns. Three definitions of cross-polarization are explained by Ludwig in the literature [15]. However, analysis of reflector antennas and feeds commonly use his third definition.

$$\eta_{pol} = \frac{P_{co}}{P_{rad}} = \frac{\int_0^{\theta_0} |C_p(\theta)|^2 \sin\theta d\theta}{\int_0^{\theta_0} [|C_p(\theta)|^2 + |X_p(\theta)|^2] \sin\theta d\theta} \quad (2.3.10)$$

where $C_p(\theta)$ is the co-polarization, and $X_p(\theta)$ is cross-polarization.

2.3.4 The phase efficiency η_ϕ :

The phase efficiency represents the uniformity at the phase of the field across the aperture plane. It depends on the relative position of the feed to the focal point of the reflector. Phase

efficiency affects the gain and side lobes, and it can be computed in terms of the co-polarized fields as [11]:

$$\eta_\phi = \frac{\left| \int_0^{\theta_0} C_p(\theta) \tan\left(\frac{\theta}{2}\right) d\theta \right|^2}{\left[\int_0^{\theta_0} |C_p(\theta)| \tan\left(\frac{\theta}{2}\right) d\theta \right]^2} \quad (2.3.11)$$

2.3.5 The surface error efficiency η_r :

η_r is independent of the feeds illumination. It is associated with far-field cancellations arising from phase errors in the aperture field caused by errors in the reflector's surface. If δ_p is the root mean square error(rms) on the surface of the reflector, the surface-error efficiency is given by [16][8]:

$$\eta_r = e^{\left(\frac{-4\pi\delta_p}{\lambda}\right)^2} \quad (2.3.12)$$

2.4 Summary

The design of a reflector antenna should start with typical elementary steps such as:

- Choose the size of the reflector based on the absolute gain or beamwidth requirements against the cost and physical limitations such as weight.
- Select a symmetric or offset configuration by considering the complexity against the performance advantage of the offset design.
- The efficiency should then be optimized by selecting a suitable feed to illuminate the dish and by the choice of edge taper where one varies the reflector parameters, such as the focal length to best suit the available feed.
- In the case of a dual reflector, the aperture distribution can be further be controlled by shaping the paraboloid and the sub-reflector. Shaped reflectors allow the aperture efficiency to be enhanced over a parabolic reflector by using a ray-optical approach to spread or concentrate the aperture energy needed.

Chapter 3

High-frequency Methods for Reflector Antennas

Introduction

DUAL reflector antennas are structurally and practically difficult to deal with because of the number of geometrical parameters. However, they still have large areas of application when high gain is desired. Several methods are available for the analysis of their characteristics, which will depend upon the desired results, i.e, the methods applied depend upon the size or the working frequency of the antenna. Recent computer development has made computer-aided design the usual practice for the investigation of antenna properties. This chapter highlights the high-frequency methods for the calculation of antenna patterns. These methods are generally used for antenna structures much larger than a wavelength. High frequency methods can be divided into two parts. Geometrical Optics, based on field distribution is described in section 3.2 and section 3.3 highlighted Physical Optics described, which is based on the current distribution. Both methods are limited by the diffraction effects which occur on the aperture edges of the reflector. This phenomenon can be analysed using the *Geometrical Theory of Diffraction* or the *Physical Theory of Diffraction*. Including these effects for the analysis, then section 3.4.2 and 3.4.3 respectively describe the extension of these 2 high-frequency techniques. Section 5 highlights the comparison between these two techniques in the Plane Wave Spectrum method, based on the Fast Fourier Transform.

3.1 Radiation structures

A voltage connected to a radiating feed source creates a surface current density. This current density creates an electromagnetic wave, which radiates into free space in the case of a transmitter. For a reflector antenna, this radiation might also originate from the aperture

plane of the paraboloid.

3.1.1 Radiation current source

The electromagnetic radiation is predicted by Maxwell's equations for harmonic time-varying fields. These following equations are the solutions represented in differential form and applying the Stokes' theorem [17][18].

$$\nabla \times \bar{E} = -J_m - jw\bar{B} \quad (3.1.1)$$

$$\nabla \times \bar{H} = J + jw\bar{D} \quad (3.1.2)$$

$$\nabla \cdot \bar{B} = \rho_m \quad (3.1.3)$$

$$\nabla \cdot \bar{D} = \rho \quad (3.1.4)$$

\bar{E} and \bar{H} are the vector electric and magnetic field intensities. B is the magnetic flux density and D represents the electric flux density.

Equations (3.1.1) and (3.1.2) are the Maxwell's equations derived from Faraday's and Ampere's Law respectively. J_m and J are the magnetic and electric conduction current densities respectively, the angular frequency with $w = 2\pi f$. ρ_m is a fictitious magnetic charge density and ρ is the electric charge density.

The radiation electric field away from the source can be computed over the current distribution on the surface. This concept helps in the calculation of the electric or magnetic field using $\bar{E} = -\nabla V$. It is convenient also to define an electric or magnetic potential vector to compute the magnetic or electric fields respectively. The differential equations for each vector can be written as [16]:

$$\bar{A} = \frac{\mu}{4\pi} \int_V \bar{J}_{es} \frac{e^{-jkR}}{R} ds' \quad (3.1.5a)$$

$$\bar{A}_m = \frac{\epsilon}{4\pi} \int_V \bar{J}_{ms} \frac{e^{-jkR}}{R} ds' \quad (3.1.5b)$$

where \bar{A} and \bar{A}_m are, respectively, the electric and magnetic vector potentials, \bar{J}_{es} and \bar{J}_{ms} are the electric and magnetic current densities and the volume at which charge and

Chapter 3. High-frequency Methods for Reflector Antennas

current densities are nonzero. k is the wave number which is related to the wavelength λ .

$$k = \frac{2\pi}{\lambda} = w\sqrt{\mu\epsilon} \quad (3.1.6)$$

Figure 3.1 shows that the distance from the integration point to the point where fields are observed is R' , where $R' = |\bar{R} - \bar{R}_i|$. The distance between the origin and the point of observation is \bar{R} , and \bar{R}_i is the point of integration.

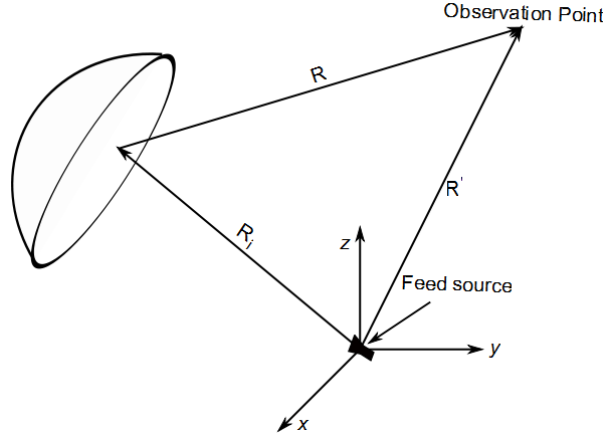


Figure 3.1: Distribution of currents on a reflector surface

The corresponding electric and magnetic fields can be written [19]:

$$\bar{E} = \frac{1}{jw\epsilon} [k^2\bar{A} + \nabla(\nabla \cdot \bar{A})] - \frac{1}{\epsilon}\nabla \times \bar{A}_m \quad (3.1.7a)$$

$$\bar{H} = \frac{1}{jw\epsilon} [k^2\bar{A}_m + \nabla(\nabla \cdot \bar{A}_m)] + \frac{1}{\mu}\nabla \times \bar{A} \quad (3.1.7b)$$

Replacing the expression of the electric and magnetic vector potential in eqs. (3.1.5b) and (3.1.5b), the solution from equations above can be expressed in terms of current densities

in the far and near fields:

$$\begin{aligned} \bar{E}(R') = & -\frac{k^2}{4\pi} \int_V [\bar{J}_{ms} \times \hat{R} \left(\frac{j}{kR} + \frac{1}{k^2 R} \right)] e^{-jkR} ds' + \\ & \frac{k^2 \eta}{4\pi} \int_V [\bar{J}_{es} \left(-\frac{1}{kR} - \frac{1}{k^2 R^2} + \frac{j}{k^3 R^3} \right) \\ & + [\bar{J}_{es} \cdot \hat{R}] \hat{R} \left(\frac{j}{kR} + \frac{3}{k^2 R^2} - \frac{3j}{k^3 R^3} \right)] e^{-jkR} ds' \end{aligned} \quad (3.1.8a)$$

$$\begin{aligned} \bar{H}(R') = & \frac{k^2}{4\pi} \int_V [\bar{J}_{es} \times \hat{R} \left(\frac{1}{kR} + \frac{1}{k^2 R} \right)] e^{-jkR} ds' + \\ & \frac{k^2}{4\pi \eta} \int_V [\bar{J}_{ms} \left(-\frac{1}{kR} - \frac{1}{k^2 R^2} + \frac{j}{k^3 R^3} \right) + \\ & [\bar{J}_{ms} \cdot \hat{R}] \hat{R} \left(\frac{j}{kR} + \frac{3}{k^2 R^2} - \frac{3j}{k^3 R^3} \right)] e^{-jkR} ds' \end{aligned} \quad (3.1.8b)$$

where,

$$\hat{R} = \frac{R - R_i}{|R - R_i|} = \frac{R - R_i}{R'} \quad (3.1.9)$$

Only the terms with $1/R$ are taken into account in the far-field terms because at a distance far from the source, terms in $1/R^2$ or $1/R^3$ will tend to zero. The radiative near-field terms depend on $1/R^2$ terms, and near-fields terms have $1/R^3$ terms dependence. η is the intrinsic (or wave) impedance ($\eta = 377\Omega$ in free space).

3.1.2 Aperture distribution source

Parabolic reflector antennas can be analysed as aperture antennas by assuming that their surface is infinitely flat. The radiation far field can be computed from the electric and magnetic fields over the aperture. The closed reflecting surface is divided by the aperture plane into two spaces, as depicted in Figure 3.2; the one containing the source is called the half-space and the second part is the free-source, where the radiation is calculated [20].

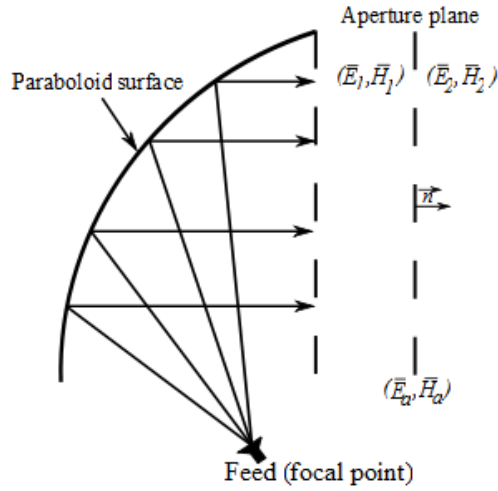


Figure 3.2: Radiation fields on a reflector aperture plane

Huygen's principle, as discussed in [10][16][21], is applied to calculate the radiation fields on the aperture plane, viz, the incident field in the aperture is replaced by an equivalent magnetic and electric source on a closed surface and this equivalent source is assumed to be zero outside the surface. This new current source can be expressed mathematically as:

$$\bar{J}_{es} = \hat{n} \times \bar{H} = \hat{n} \times (\bar{H}_2 - \bar{H}_1) \quad (3.1.10a)$$

$$\bar{J}_{ms} = -\hat{n} \times \bar{E} = -\hat{n} \times (\bar{E}_2 - \bar{E}_1) \quad (3.1.10b)$$

where \bar{H}_1 and \bar{E}_1 represent the tangential magnetic and electric fields on the first region (region 1); \bar{H}_2 and \bar{E}_2 are fields on region 2 and \hat{n} is the unit vector normal to the surface. The parabola surface is assumed to be an infinite plane, and if fields (\bar{E}, \bar{H}) on the first region are chosen to be zero, then, currents in (3.1.10a) and (3.1.10b) are calculated on the boundary and can be expressed in term of the aperture magnetic and electric field as:

$$\bar{J}_{es} = \hat{n} \times \bar{H}_a \quad (3.1.11a)$$

$$\bar{J}_{ms} = -\hat{n} \times \bar{E}_a \quad (3.1.11b)$$

The radiation pattern of reflector antennas can either be computed from the distribution of surface currents on the reflectors, or from the prime reflector aperture field, by considering the reflector antenna as an aperture radiator. These methods are called, respectively, the current distribution method and the aperture distribution method. These methods are specified as an asymptotic high frequency method and ignore the diffraction effects on the reflector surface.

3.2 Geometric Optics theory

Geometrical optics or the *ray optics* technique is based on the aperture distribution assumption, to compute the propagation wave for the incident, reflected and the refracted fields. Maxwell's equation's prediction of the electromagnetic wave is related to the Geometrical Optics as discussed in [22]. The GO method is accurate for analysing or designing reflector antennas, since they have large dimensions compared to the wavelength. Then, too, its approximation cost is independent of the size of the structure and its accuracy improves as structure size increases.

The classical geometrical optics starts from *Fermat's principle*. Fermat's principle states that the path of a light ray follows is an extremum in comparison with the nearby paths. The optical path length is defined as [23]:

$$\delta \int_{P_0}^{P_1} n(s) ds \quad (3.2.1)$$

where P_0 and P_1 are the extremum, δ represents the calculus variation and $n(s)$ is the index of refraction of the medium, which is a function of position along the path between points P_0 and P_1 . In a homogeneous medium, the rays are straight lines wherein the index of refraction is constant.

$$n(s) = \sqrt{\frac{\mu\epsilon}{\mu_0\epsilon_0}} \quad (3.2.2)$$

The solution of the electric and magnetic fields from the exact electromagnetic theory can be expanded into power series in inverse powers of the angular frequency ω [24][25].

$$\bar{E}(R', \omega) = e^{-jk_0 L(R')} \sum_{m=0}^{\infty} \frac{\bar{E}_m(R')}{(j\omega)^m} \quad (3.2.3a)$$

$$\bar{H}(R', \omega) = e^{-jk_0 L(R')} \sum_{m=0}^{\infty} \frac{\bar{H}_m(R')}{(j\omega)^m} \quad (3.2.3b)$$

where $L(R')$ is called the optical path length or *eikonal* and $k_0 = \sqrt{\mu_0\epsilon_0}$ is the propagation constant in the vacuum. The equiphase wave fronts are given by the level surfaces of the eikonal function. The polarisation, the phase and wavelength are not taken into account in the classical geometric optics. The extension of this technique can be done by using the asymptotic solution of the Maxwell's equation as $\omega \rightarrow \infty$.

$$\bar{E}(R', \omega) \approx \bar{E}_0(R') e^{-jk_0 L(R')} \quad (3.2.4a)$$

$$\bar{H}(R', \omega) \approx \bar{H}_0(R') e^{-jk_0 L(R')} \quad (3.2.4b)$$

In geometric optics, the eikonal equation came from the solution of the Maxwell's equation, which is expressed in form [23]:

$$|\nabla \bar{L}(R')|^2 = n^2 \quad (3.2.5)$$

where the function $\bar{L}(R')$ must satisfy the differential equation:

$$|\nabla L|^2 = \left(\frac{\partial L}{\partial x}\right)^2 + \left(\frac{\partial L}{\partial y}\right)^2 + \left(\frac{\partial L}{\partial z}\right)^2 = n^2 \quad (3.2.6)$$

3.2.1 Propagation of rays in Geometrical Optics

The principle of GO can be proved by computing a secondary wave front surface L_n after a short time $t = t_{n+1} > t_n$ with $(n = 0, 1, 2, \dots)$, from a primary wave front surface L_0 at t_0 , as illustrated in Figure 3.3. This secondary wave front is a straight line for an homogeneous medium. However, it has a curvature in an inhomogeneous medium.

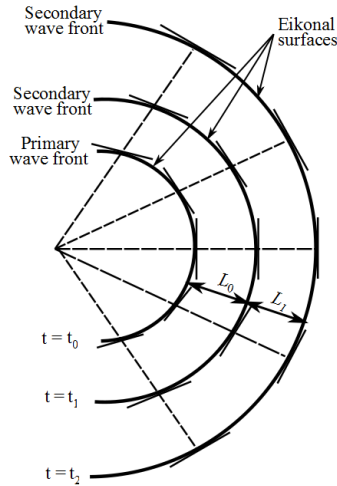


Figure 3.3: Primary and secondary wave of radiated wave after [24].

Since the rays in the medium move in a velocity equal to the velocity of light, the phase increases between the 2 successive surfaces $(\omega/c)\delta L$, while the wave traverses from one surface to another with a time difference $\delta t = t_1 - t_0$. Then, the secondary wave front L_1 is described from the connection of the surface normal to each of the rays [24].

The wave fronts are defined by letting the function $L(R')$ equal a constant. The local wave vector $\nabla \bar{L}(R')$ evaluated at any point in space is always normal to the wave front passing through it. The direction of the ray can be expressed as [26].

$$\hat{s} = \frac{\nabla L}{n} \quad (3.2.7)$$

where \hat{s} is the unit vector normal to the wave front. The fields at any point over a ray are perpendicular to the ray.

3.2.2 Reflection on the boundary

To enhance the use of geometric optics, it is more important to define the behaviour of the ray on the boundary, rather than determining the geometrical optics properties of rays through the surface. In geometrical optics, the direction of the fields is defined by the ray equation. Let $\bar{r}(s)$ be the position vector of the ray over the path and, since $\hat{s} = d\bar{r}/ds$, the equation can be written from (3.2.7) as [26]:

$$\frac{d^2\bar{r}}{ds^2} = \frac{d\bar{r}}{ds} \cdot \nabla \left(\frac{d\bar{r}}{ds} \right) = \hat{s} \cdot \nabla(\hat{s}) = \frac{\nabla L}{n} \cdot \nabla \left(\frac{\nabla L}{n} \right) \quad (3.2.8)$$

In an homogeneous medium this equation is equal to zero, at which the wave front is a straight line.

$$\frac{d^2\bar{r}}{ds^2} = \frac{1}{2} \nabla \left(\frac{|\nabla L|^2}{n^2} \right) = 0 \quad (3.2.9)$$

At the boundaries, as the 2 mediums differ from each other in their reflective indexes respectively, n_1 and n_2 , as illustrated in Figure 3.4, the behaviour of the ray follows Snell's Law. The equation (3.2.8) is integrated at the point of reflection, where the tangential component of the rays is vanishing, thus the incident ray is related to the reflected. Applying Stoke's theorem and assuming that the boundary surface is for $\delta \rightarrow 0$.

$$\iint d\bar{S} \cdot \nabla \times (\hat{s}n) = \oint_C d\bar{l} \cdot \hat{s}n = 0 \quad (3.2.10)$$

where $d\bar{l}$ is the differential line over the closed reflection surface and $d\bar{S}$ is the unit vector normal to the surface.

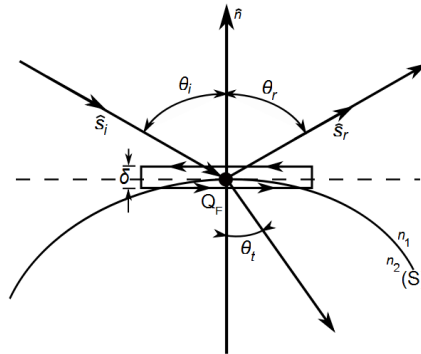


Figure 3.4: Derivation from Snell's Law: the unit vector \hat{s}_i is in the direction of the incident ray and \hat{s}_r is in the direction of the reflected ray after [24]

From Snell's principle, the transmitted and reflected ray are:

$$n_1 \sin \theta_i = n_2 \sin \theta_t \quad (3.2.11)$$

and at the reflection region, the indexes of refraction are identical ($n_1 = n_2$). From Figure 3.4, the angle of reflection is $\theta_t + \theta_r = \pi$. Therefore the relation between the incident and reflected angles is:

$$n_1 \sin \theta_i = n_1 \sin \theta_r \quad (3.2.12)$$

3.2.3 Propagation power of the rays

In geometric optics, the power per unit solid angle between two points is influenced by the conservation of energy flux in a tube of rays [24]. The total power within the cross section of the flux tube must be constant since power propagates in the direction of the rays only. When the flux tube cross section dA_0 and power density S_0 are known at a reference point and the flux tube cross section area dA is known, then the radiation density S is given in terms of S_0 as:

$$S_0 dA_0 = S dA \quad (3.2.13)$$

Radiation densities S and S_0 are assumed constant throughout the cross section areas dA_0 and dA respectively, thus no power flows across the side of the tube [8]. For the electromagnetic wave, the time average Poynting vector can be written as [26]:

$$\begin{aligned} \bar{S} &= \frac{1}{2} \text{Re} \bar{E} \times \bar{H}^* = \frac{1}{2n\eta} \text{Re} \bar{E} \times (\nabla L \times \bar{E})^* \\ &= \frac{1}{2n\eta} (\bar{E} \cdot \bar{E})^* \nabla L \\ &= \hat{s} \frac{1}{2\eta} |\bar{E}|^2 \end{aligned} \quad (3.2.14)$$

3.3 Physical Optics theory

Physical Optics (PO) or *wave optics* is one of the high frequency methods commonly used for reflector antenna analysis because of its accuracy. It is based on current distribution method by using Huygen's principle as discussed in §3.1.1.

3.3.1 Induced current density for PEC

The principle of PO is to integrate the induced current distribution on the reflector surface. Considering the surface as a perfect conductor, the induced current density is the composition of the incident and reflected tangential magnetic fields on the surface. Ignoring the contribution of current on the reflector shadowed region and the tangential component, the H -field on the surface is doubled on the illuminated region, according to the method of images [27][24]. Assuming the reflecting surface to be locally plane, the physical optics current density for a PEC ($\hat{n} \times \bar{H}^i = \hat{n} \times \bar{H}^r$) is given by:

$$\bar{J}_s = \begin{cases} \hat{n} \times (\bar{H}^i + \bar{H}^r) & ; \text{ illuminated region} \\ 0 & ; \text{ shadowed region} \end{cases} \quad (3.3.1)$$

or

$$\bar{J}_s = \begin{cases} 2\hat{n} \times \bar{H}^i & ; \text{ illuminated region} \\ 0 & ; \text{ shadowed region} \end{cases} \quad (3.3.2)$$

where \bar{H}^i and \bar{H}^r are the incident and reflected magnetic fields computed across the surface. In case of a dual reflector, the radiation field may radiate from the feed source or be scattered from the sub-reflector. The PO technique can account for diffraction, interference and polarization effects, as well as aberrations and other complex effects.

The radiation current density approximation represented in (3.3.2) is defined as the *Physical Optics approximation*. It is valid only for large electrical size antenna structures, i.e. either the radius of curvature of the reflector or the radius of curvature of the incident wave are greater than about 5λ [27][28].

3.3.2 PO radiation fields

The radiation fields scattered on the reflector surface can be computed using eqs. (3.1.8a) and (3.1.8b). The PO current over the surface is assumed to be constant in amplitude and phase, the radiation integral is then reduced to a simple summation [16]. From (3.1.8b), the magnitude of the magnetic field over a conducting surface is:

$$H(R_i) = -\frac{1}{4\pi} \int_{\Sigma} \left(jk + \frac{1}{R'} \right) \hat{R} \times J_s(R_i) \frac{e^{-jkR'}}{R'} ds \quad (3.3.3)$$

Computation is simplified by replacing the reflector surface Σ by an adjacent N -plane rectangular facet Δ_k , where $k = 1, \dots, N$ corresponds with the triangle. Replacing the

surface \sum by the triangle facet, then (3.3.3) becomes [29]:

$$H(R_i) = -\frac{1}{4\pi} \sum_{k=1}^N \left(jk + \frac{1}{R'_k} \right) \hat{R}_k \times T_k(R_i) ds \quad (3.3.4)$$

in which,

$$T_k(R_i) = \int_{\Delta_k} J_k(R_i) \frac{e^{-jkR'}}{R'} ds \quad (3.3.5)$$

and the PO surface current on the surface can be expressed in terms of the incident field H_s .

$$J_k(R_i) = 2\hat{n}_k \times H_s(R_i) \quad (3.3.6)$$

3.3.3 Dual-reflector application

PO technique is commonly used for dual reflector antenna analysis because of its accuracy. Firstly, as the radiation feed source illuminates the sub-reflector, the induced current on the sub-reflector is computed. Subsequently, the near field scattered from the sub-reflector becomes a new source to illuminate the main reflector, and its far field scattered is determined from the integration of the induced current over the reflector. The complexity of this method is revealed by the use of the various coordinate systems of the structure as illustrated in Figure 3.5.

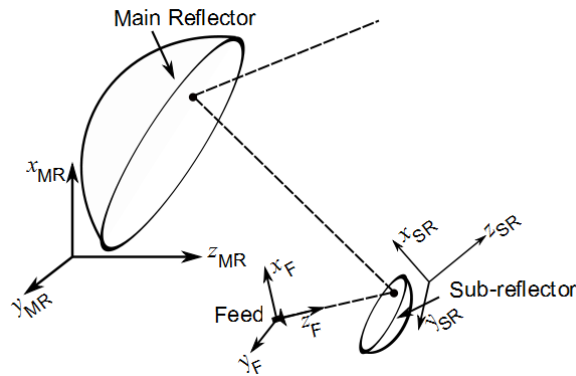


Figure 3.5: Offset Gregorian dual reflector coordinate system after [30]

3.4 Analysis of the diffraction effect on the sub-reflector rim

3.4.1 Huygens-Fresnel principle of diffraction

One of the most difficult problems to solve in optics is the diffraction phenomenon. Diffraction theory is based on the *Huygens-Fresnel principle*. According to Huygens' construction, every point on a primary wave-front serves as a source of secondary spherical wavelets, such that the primary wave-front is the envelope of these wavelets in a subsequent time (see Figure 3.6). Moreover, the wavelets advance with a speed and frequency equal to those of the primary wave at each point in space. This principle was further added to Fresnel, where the superposition of the secondary wave-front takes into account the amplitude and phase of the wavelets [31].

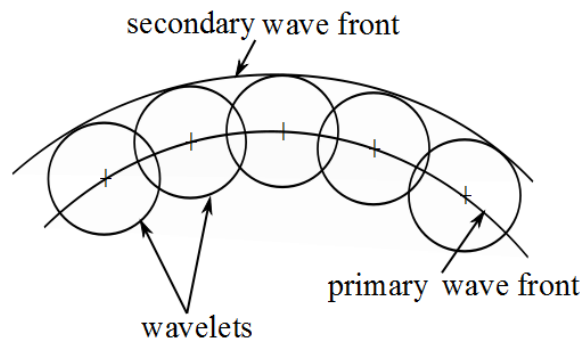


Figure 3.6: Huygens geometry construction

The GO described earlier is used to determine the scattering field in the illuminated region but cannot predict the non-zero field in the shadow. However, the analysis of diffraction on the parabolic reflector edges or rim will permit the computation of the field in the shadow region as illustrated in Figure 3.7. Wave diffraction in space is a local phenomenon at high frequency, hence the field value of the diffracted rays is proportional to the field value of the incident rays at the point of diffraction multiplied by a coefficient called the *diffraction coefficient* [8].

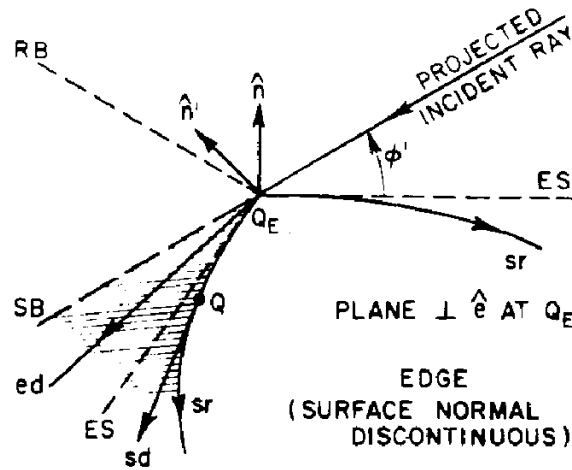


Figure 3.7: Rays diffracted in the parabolic reflector edges [32][23].

where Q_E is the diffraction point, the incident rays to the edge forms the edge diffracted field ed and the surface diffracted field sr . ES is the boundary between between ed and sr and tangent to the surface on Q_E . RB and SB define the shadow boundaries of the incident and reflected field, respectively.

The computation of this diffraction coefficient depends strictly on the properties of the waves and the boundary where the point of diffraction is considered. The complex geometries of reflector antennas are approximated with the help of *canonical* problems to investigate the diffracted field, where the exact edge geometry is simplified by this canonical problem. This simple model is then used to calculate the diffracted field. The surface edge geometry is defined for a canonical problem and the examination is reduced into a half plane problem for analysis of a cylindrical reflector antenna.

3.4.1.1 Edge diffraction in the sub-reflector surface

The electromagnetic wave from the feed source illuminates the ellipsoid sub-reflector surface, and the total electric field E_{tot} is the sum of the incident field from the source E_i and the radiated field from the reflector E_r for a finite size antenna. However, in a discontinuous medium such as an edge, the field on the shadowed region is not negligible according to Huygens source. The total field in the aperture is given for this case as [23]:

$$\vec{E}_{tot} = \vec{E}_i u_i + \vec{E}_r u_r + \vec{E}_d \quad (3.4.1)$$

where \vec{E}_d is the edge diffracted field. The GO method can evaluate directly \vec{E}_i and \vec{E}_r ; and the diffraction integral is applied for \vec{E}_d resolution.

The analysis of reflector antennas results in a great improvement performance when accounting the diffraction on the edge. The following sections describe the extension of the

PO and GO methods, respectively called PTD or *Physical Theory of Diffraction* and GTD or *Geometric Theory of Diffraction*.

3.4.2 Geometrical Theory of Diffraction

An incoming incident rays striking an edge surface boundary creates non-uniform diffracted rays. Either PTD or GTD are, respectively, techniques used to describe this diffraction phenomena at a particular region called the *shadow*, wherein, the electric field is assumed to be zero for the ordinary GO.

3.4.2.1 Geometrical Optics fields

The GTD presented in this section is an assumption technique developed by Keller in 1950s for the extension of GO as described in [33]. To make use of the efficiency of GO, Keller took into account the diffracted ray in the shadow region; however the GTD is still limited because of the non-uniformity of the diffracted fields on the transition region surrounding the surface boundary [34]. Keller's conception is based on Fermat's principle, and investigates the diffraction point location and the orientation of the diffracted rays propagation.

3.4.2.2 Diffracted fields on a curved surface

Figure 3.8 represents the diffraction at the curved surface edge. For an oblique incident ray having an angle β_0 on the edge, the diffracted field lies on the surface of a cone with an angle $\beta_0/2$. The diffracted electric field on the surface is expressed as [23]:

$$E_d(s) = E_i(Q_E) \cdot \overline{D}(\phi, \phi', \beta_0) A(s) e^{(-jks)} \quad (3.4.2)$$

where $E_i(Q_E)$ is the incident field at the point of diffraction Q_E , $\overline{D}(\phi, \phi', \beta_0)$ is the dyadic diffraction coefficient for a perfect conducting wedge.

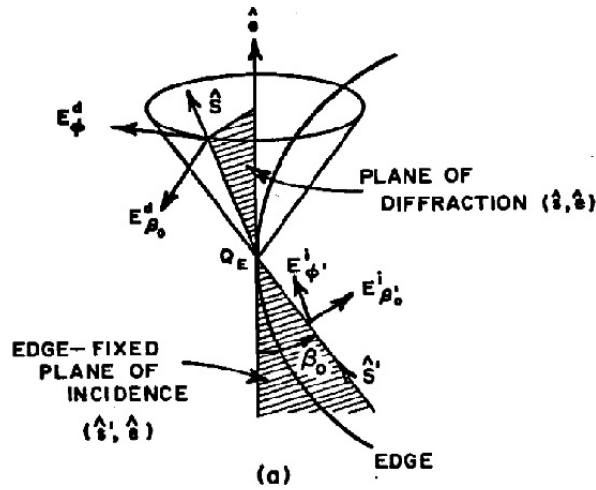


Figure 3.8: Diffracted at a curved edge [24].

Then, the spacial attenuation factor or spreading factor $A(s)$, which is defined as the variation of the field intensity along the diffracted ray, for an incident spherical wave is given as [24]:

$$A(s) = \sqrt{\frac{\rho}{s(\rho + s)}} \approx \frac{\sqrt{\rho}}{s} \text{ for } s \gg \rho \quad (3.4.3)$$

where s is the distance from the diffraction point to the field observation point and the ρ is the distance between the caustic at the edge and the second caustic of the diffracted ray. The caustic distance ρ is related to the normal incidence β_0' as [35]:

$$\frac{1}{\rho} = \frac{1}{\rho_e} - \frac{\hat{n}_e \cdot (\hat{s}' - \hat{s})}{a \sin^2 \beta_0} \quad (3.4.4)$$

in which,

ρ_e is the radius of curvature of the incident wave front at the point of diffraction taken into the plane of the incident ray, containing the unit vectors \hat{s}' and \hat{e} ;

a is the radius of curvature of the edge at the point of diffraction Q_E , and

\hat{n}_e is the unit normal vector to the edge directed away from the centre of curvature.

From Figure 3.8, the unit vectors $\hat{\beta}_0'$ and $\hat{\beta}_0$ are related respectively by:

$$\hat{\beta}_0' = \hat{s}' \times \hat{\phi}' \quad (3.4.5a)$$

$$\hat{\beta}_0 = \hat{s} \times \hat{\phi} \quad (3.4.5b)$$

Chapter 3. High-frequency Methods for Reflector Antennas

The diffracted field is obtained from the dyadic diffraction coefficient at the edge. This diffraction coefficient can be described by:

$$\bar{D}(\phi, \phi'; \beta_0) = -\hat{\beta}'_0 \hat{\beta}_0 D_s(\phi, \phi'; \beta_0) - \hat{\phi}' \hat{\phi} D_h(\phi, \phi', \beta_0) \quad (3.4.6)$$

where D_s and D_h are, respectively, the scalar diffraction coefficient for the soft boundary condition (Dirichlet) and the scalar diffraction coefficient for the hard (Neumann) boundary condition at the edge. They can be represented respectively by:

$$D_s(\phi, \phi'; \beta_0) = D_i(\phi, \phi'; \beta_0) - D_r(\phi, \phi'; \beta_0), \quad (3.4.7a)$$

$$D_h(\phi, \phi'; \beta_0) = D_i(\phi, \phi'; \beta_0) + D_r(\phi, \phi'; \beta_0) \quad (3.4.7b)$$

where

$$\begin{aligned} D_{i,r}(\phi, \phi'; \beta_0) = & -\frac{e^{-j\pi/4}}{2n\sqrt{2\pi\beta\sin\beta'_0}} \\ & \times \left\{ \cot\left[\frac{\pi + (\phi + \phi')}{2n}\right] F[kL^i a^+(\phi - \phi')] \right. \\ & + \cot\left[\frac{\pi - (\phi - \phi')}{2n}\right] F[kL^i a^-(\phi - \phi')] \\ & \mp \left\{ \cot\left[\frac{\pi + (\phi + \phi')}{2n}\right] F[kL^{rn} a^+(\phi - \phi')] \right. \\ & \left. \left. + \cot\left[\frac{\pi + (\phi + \phi')}{2n}\right] F[kL^{ro} a^-(\phi + \phi')] \right\} \right\} \quad (3.4.8) \end{aligned}$$

wherein $F(X)$ is the transition function expressed as:

$$F(X) = 2j\sqrt{X}e^{jX} \int_{\sqrt{X}}^{\infty} e^{-j\tau^2} d\tau; \quad (3.4.9)$$

and

$$a^{\pm}(\phi \pm \phi') = 2\cos^2\left(\frac{2n\pi N^{\pm} - (\phi \pm \phi')}{2}\right) \quad (3.4.10)$$

at which N^{\pm} are the integers which mostly satisfy the equations [23]:

$$2\pi n N^+ - (\phi \pm \phi') = \pi \quad (3.4.11a)$$

$$2\pi n N^- - (\phi \pm \phi') = -\pi \quad (3.4.11b)$$

where L^i and L^r are the distance parameters, which expressed as

$$L^i = \frac{s(\rho_e^i + s)\rho_1^i\rho_2^i\beta_0}{\rho_e^i(\rho_1^i + s)(\rho_2^i + s)}; \quad (3.4.12a)$$

$$L^r = \frac{s(\rho^r + s)\rho_1^r\rho_2^r\beta_0}{\rho^r(\rho_1^r + s)(\rho_2^r + s)} \quad (3.4.12b)$$

where ρ_1^i, ρ_2^i and ρ_1^r, ρ_2^r are the principal radii of curvature of the incident wavefront and the reflected wavefront at the point of diffraction Q_E respectively. Then, ρ_e^i, ρ_r^i are radii of curvature of the incident and reflected wave front at the point Q_E taken from the plane containing the incident, the reflected and diffracted ray respectively and the unit vector \hat{e} . The superscripts "o" and "n" on L^r in equation (3.4.8) indicate the radii of curvature ρ_1^o, ρ_2^o and the distance parameters ρ^o must be calculated from the "o" face and "n" face of the wedge. At the far field observation where $s \gg \rho^i, \rho_1^i, \rho_2^i, \rho^r, \rho_1^r, \rho_2^r$, eqs. (3.4.12a) and (3.4.12b) reduce into:

$$L^i = \frac{\rho_1^i\rho_2^i}{\rho_e^i} \sin^2 \beta'_0 \quad (3.4.13)$$

and

$$L^{ro} = L^{rn} = L^r = \frac{\rho_1^r\rho_2^r}{\rho^r} \sin^2 \beta'_0 \quad (3.4.14)$$

3.4.3 Physical Theory of Diffraction

The PTD or *Physical Theory of Diffraction* is an asymptotic technique developed in the 1950s by Professor Ufimtsev to overcome the diffraction issue [36]. It is an improvement of PO technique wherein the diffraction effects such as the discontinuity of the surface currents at boundaries of the illuminated and shadow regions near the edges of the surface is taken into account.

The PO current in (3.3.2) §3.3.1 is corrected by a *nonuniform* current that accounts for diffraction effects and is expressed as [37]:

$$\vec{J}_s(r) = \vec{J}_{PTD}(r) - \vec{J}_{PO}(r) \quad (3.4.15)$$

where $\vec{J}_{PO}(r), \vec{J}_{PTD}(r)$ are the PO and the PTD current contribution respectively, $J_s(r)$ is the surface current density.

Besides, the scattered field in PTD is, of course, different from that calculated using the *Geometrical Theory of Diffraction*, because it includes the "nonuniform" current or the fringing current at the surface edges. The total scattered fields resulting from the current

on the surface is given as:

$$E_{tot}^s(r) = E_{PO}^s(r) + E_{PTD}^s(r) \quad (3.4.16)$$

$E_{PO}^s(r)$ and $E_{PTD}^s(r)$ are the PO and the PTD scattered fields respectively. The computation of the scattered fields for this present method is discussed in the next paragraph.

3.4.3.1 Method of Equivalent Current

$E_{PTD}^s(r)$, called the correction term, can be calculated by using the Method of Equivalent Current (MEC). The MEC reduces the evaluation of surface integrals for the fringe surface currents to line integrals around the edges of the surface of the scatterer, as discussed in literature [38],[39]. Using MEC, the PTD scattered fields are described as:

$$E_{PTD}^s(r) = \frac{jk_0}{4\pi} \oint (\eta_0 \hat{r} \times \hat{r} \times \mathbf{I}_f + \hat{s} \times \mathbf{M}_f) \frac{-jk_0 r}{r} dl \quad (3.4.17)$$

\mathbf{I}_f and \mathbf{M}_f are the fringe electric and the magnetic equivalent edge currents respectively.

Asymptotic techniques as GTD and PTD have been performed to deal with the diffraction problem. However, they are sometimes limited by the size and the complexity of the geometry of the antenna, even though several approximations are applied to accomplish the task and to obtain the correct results.

Actually, the development of various software solutions for antenna analysis not only reduces the task of an engineer, but also standardises a low cost antenna design. Moreover, the electromagnetic problem involving particularly the scattering, propagation, radiation and acoustic fields can be also proved using a *Plane Wave Spectrum* or PWS. This method is outlined in a subsequent section.

3.5 Antenna Radiation pattern using Plane Wave Spectrum

Several methods have been developed for the resolution of electromagnetic problems. Each method has its own particular advantages. The combination of methods is actually necessary to investigate the properties of antennas with complex geometry.

Superposition of plane waves propagating in different directions with different amplitudes is called a *Plane Wave Spectrum* or an *angular spectrum* of a plane wave [1]. It is applied to compute the test zone field from a known reflector aperture field distribution. This method is accurate for the investigation of reflectors having a notched rim for reduced edge diffraction [40].

3.5.1 Plane waves spectrum representation

The properties of a plane wave travelling in a uniform, isotropic and lossless open region is described in literature [41]. Waves are said to be plane if their equi-phase surface is planar. If the equiamplitude surfaces of plane waves are also equiphases, then, they are known as *homogeneous*. Assuming that the total field satisfies the harmonic time dependence $e^{j\omega t}$, given by the homogeneous Helmholtz equation [19] [42]:

$$\nabla^2 E(x, y, z) + k_0 E(x, y, z) = 0 \quad (3.5.1)$$

where $k_0 = \omega \sqrt{\mu_0 \epsilon_0}$ is the wave number in free space. Therefore, the electric field solution of (3.5.1) can be written in terms of the angular spectrum, which is the superposition of plane waves propagating in different directions with different amplitudes:

$$E(x, y, z) = \frac{1}{4\pi^2} \int_{-\infty}^{+\infty} \int_{-\infty}^{+\infty} F(k_x, k_y, z) e^{-jk_r} dk_x dk_y \quad (3.5.2)$$

Figure 3.9 illustrated the free space propagator vector k and the position vector r are respectively and they are described by:

$$\underline{k} = k_x \hat{x} + k_y \hat{y} + k_z \hat{z} = k_0(u \hat{x} + v \hat{y} + w \hat{z}) \quad (3.5.3a)$$

$$\underline{r} = x \hat{x} + y \hat{y} + z \hat{z} \quad (3.5.3b)$$

In spherical coordinates, $u = \sin\theta \cos\phi$, $v = \sin\theta \sin\phi$ and $w = \cos\theta$ are the direction cosine.

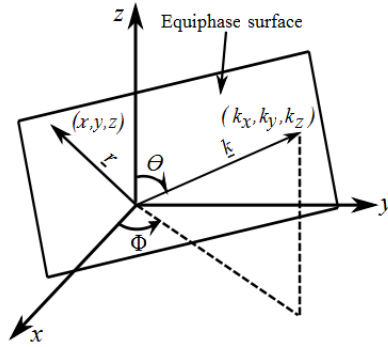


Figure 3.9: Plane wave propagation coordinate system.

By replacing the value of k and r , (3.5.2) can be written in spectral domain for $z = 0$ as [43][44]:

$$E(x, y, 0) = \frac{1}{4\pi^2} \int_{-\infty}^{\infty} \int_{-\infty}^{\infty} F(k_x, k_y) e^{-j(k_x x + k_y y)} dk_x dk_y \quad (3.5.4)$$

and the wave number in z-direction is given by:

$$k_z^2 = k_0^2 - (k_x^2 + k_y^2) \quad (3.5.5)$$

or

$$k_z = \begin{cases} +\sqrt{k_0^2 - (k_x^2 + k_y^2)}, & \text{if } k_x^2 + k_y^2 \leq k_0^2 \\ -j\sqrt{(k_x^2 + k_y^2) - k_0^2}, & \text{if } k_x^2 + k_y^2 > k_0^2 \end{cases} \quad (3.5.6)$$

when $k_x^2 + k_y^2 \leq k_0^2$, the real value of k_z will correspond with the radiation field of the aperture, k_z corresponds to the evanescent waves for $k_x^2 + k_y^2 > k_0^2$, and $F(k_x, k_y)$ is the two-dimensional angular spectrum of the field.

3.5.2 The Angular spectrum approximation

The antenna far field is approximated by the angular spectrum. The PWS method requires two general assumptions for far field antenna computation which are [1]:

- a. the aperture antenna dimensions have a finite length, wherein the field sources lying in the half-space behind the aperture plane are finite and occupy a finite volume;
- b. the \mathbf{kr} values must be large compared to the wavelength and the greatest dimension of the aperture .

The two-dimensional inverse Fourier transform integral is computed using *the method of stationary phase*, as described in literature [41][6]. The integral equation (3.5.6) is computed using this method and the radiated far field can be expressed approximately as:

$$E(r, \theta, \phi) \simeq jk \frac{e^{jkr}}{2\pi r} [\cos\theta f(k_x, k_y)] \quad (3.5.7)$$

with

$$f(k_x, k_y) = f_x(k_x, k_y)\hat{x} + f_y(k_x, k_y)\hat{y} + f_z(k_x, k_y)\hat{z} \quad (3.5.8)$$

The θ and ϕ components are dominant in the far zone field. (3.5.7) shows that the two-dimension inverse Fourier transform can be approximated into a multiplication of a normalisation constant with a trigonometric function. Despite this fact (3.5.7) is valid for only some values of stationary points which can be described as:

$$k_x = k_0 \sin\theta \cos\phi \quad (3.5.9a)$$

$$k_y = k_0 \sin\theta \sin\phi \quad (3.5.9b)$$

$$k_z = k_0 \cos\theta \quad (3.5.9c)$$

The E_θ and E_ϕ component can then be written as:

$$E_\theta(r, \theta, \phi) \simeq jk \frac{e^{jkr}}{2\pi r} (f_x \cos\theta + f_y \sin\phi) \quad (3.5.10a)$$

$$E_\phi(r, \theta, \phi) \simeq jk \frac{e^{jkr}}{2\pi r} (-f_x \sin\theta + f_y \cos\phi) \quad (3.5.10b)$$

3.6 Conclusion

In this chapter a brief overview of some high frequency asymptotic techniques from CEM theory are presented. It is shown that the diffraction limitations of the GO and PO techniques can be corrected for by including the diffraction term analysis using the PTD and GTD extension methods. These are based on the physical and geometrical assumption respectively and are accurate for electrically large antennas. These two techniques used often for computer-aided applications because they produce favourable memory and runtime results. Even if several approximations are assumed for the dual reflector antenna analysis, these high-technique methods are restricted by the complexity of the dual reflector antenna geometry.

Chapter 4

Description of a Gregorian Reflector Antenna and Creation of a FEKO Reference

Introduction

A Reflector antenna with a low polarization and side lobe level is difficult to engineer because of the aperture blockage or scattering of the feed or sub-reflector. An offset antenna is a most interesting structure employed to avoid not only this blockage, but also the multiple reflections between the feed and reflectors, although an increase of cross polarization is the penalty.

This chapter highlights a description of a classical offset dual reflector; section 4.1 shows the geometry structure for a particular type of offset reflector, section 4.1.5 describes parameters of the design and section 4.2.1 investigates the feed system.

The full antenna radiation properties are computed using a numerical method, based on a combination of Method of Moments (MoM) and the Physical Optics high frequency technique using a software package FEKO in section 4.2. This technique is suitable for accurate analysis of an offset dual reflector antenna when the following is done: an analytical function is used to approximate the pattern of the feed, and the antenna system is then subdivided into two parts with ; the MoM applied for the small sub-reflector and PO for the main reflector.

4.1 Description of the Gregorian Reflector Antenna

4.1.1 Gregorian geometry structure

An offset Gregorian reflector antenna is a paraboloidal reflector with a concave sub-reflector of ellipsoidal shape, located at a distance from the vertex of the prime reflector, that distance being greater than the prime focal distance of the main reflector. The system offers several significant advantages over its axis-symmetric counterpart for many applications, such as remote sensing, satellite communications, radio astronomy, etc. Figure 4.1 depicts the geometric structure of this antenna and its parameters are described in Table 4.1.

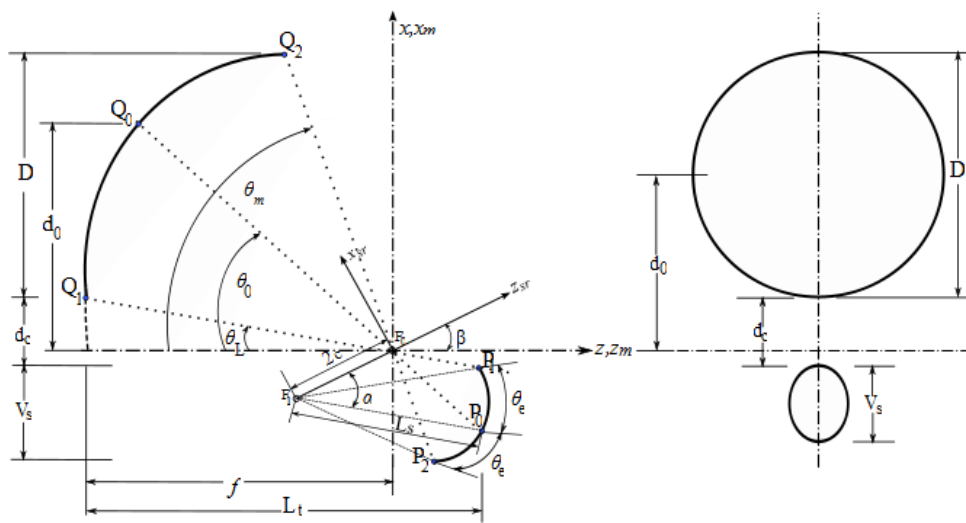


Figure 4.1: Front and side view of a Gregorian dual reflector after [45]

F_0 and F_1 are the foci of the ellipsoid sub-reflector. F_0 is pointed at the prime reflector focal point and the feed source is placed at F_1 . Rays from F_1 are reflected by the sub-reflector. Reflected rays will emanate the main reflector through F_0 .

$(0, x_{sr}, z_{sr})$ is the sub-reflector axis and $(0, x_m, z_m)$ defines the main reflector axis, which is situated at the system axis $(0, x, z)$. These two axes are tilted at an angle β . Angles are considered positive if the rotation on the y axis is counterclockwise, and negative if in the opposite direction [46], except for the angle θ_e on the sub-reflector, which is always positive.

Table 4.1: Gregorian design parameters

Parameter	Description
D	Diameter of the main reflector on the xy plane
f	Focal length of the parabolic main reflector
d_0	Distance between the point Q_0 on the main and the sub-reflector z axis
d_c	Minimum vertical distance between the main and the sub-reflector edges along x axis
θ_0	Offset angle of the main reflector
θ_m	Offset angle at the top of the main reflector
θ_L	Offset angle at the bottom angle of the main reflector
β	Tilt angle between the sub- and main reflector
e	eccentricity of the ellipse ($0 < e < 1$)
θ_e	Half-angle subtended by the sub-reflector as viewed from the focal point F_1
a	Surface parameter of the sub-reflector
c	Half interfocal distance
α	Tilt angle between the sub-reflector and the feed
V_s	Sub-reflector projection height
L_t	Maximum length of the antenna system along the x axis
L_s	Distance between the focal point and the point P_0 on the sub-reflector
L_{sr}	Maximum diameter of the sub-reflector
L_m	Distance between the sub-reflector point P_0 and the point Q_0 on the main reflector

4.1.2 Main Reflector

4.1.2.1 Characteristics of the Main Reflector

The prime reflector has a circular aperture when projected on the aperture plane. It is described by the diameter D of the paraboloid, the focal length f , and offset distance d_0 . In Figure 2.4, f represents the focal length of the paraboloid with the origin located on the second focal point F_0 , ρ_m is the distance from that focal point F_0 into the paraboloid surface point and θ is the offset reflector angle.

4.1.2.2 Main reflector parameters

The offset angle of the main reflector has three different values, which are: θ_0 , the angle from the main reflector z -axis into the centre of the paraboloid surface and, θ_L , θ_m , the bottom

Chapter 4. Description of a Gregorian Reflector Antenna and Creation of a FEKO Reference

and the top angle respectively. From Figure 4.1 the equation can be written:

$$\tan\left(\frac{-\theta_0}{2}\right) = \frac{d_0}{2f} \quad (4.1.1a)$$

or

$$\theta_0 = -2\arctan\left(\frac{d_0}{2f}\right) \quad (4.1.2a)$$

The bottom and the top offset angle of the main reflector can be derived from (4.1.2a) as:

$$\theta_L = -2\arctan\left(\frac{d_0 - \frac{D}{2}}{2f}\right) \quad (4.1.3a)$$

$$\theta_m = -2\arctan\left(\frac{d_0 + \frac{D}{2}}{2f}\right) \quad (4.1.3b)$$

D is the diameter of the main reflector and d_0 is the clearance between the top of the sub-reflector and the bottom of the main reflector. The negative sign indicates that the orientation of the angle is counterclockwise.

4.1.3 Sub-reflector

4.1.3.1 Characteristics of the sub-reflector

A sub-reflector that has an elliptical aperture is described by its projected height V_s , the tilt angle between the main reflector and sub-reflector axis β , interfocal distance $2c$, and eccentricity e , as listed in Table 4.1.

The feed parameters are the sub-reflector edge angle θ_e , as observed from the reflector system focus, and the feed pointing angle α ; and L_t is the total length of the antenna system. The ellipse is the locus of points for which the sum of the distances from two given points, viz the foci, is constant and equal to $2a$; where a is the major radius of the ellipse ($F_1P_0 + F_0P_0 = 2a$). Thus the surface of the ellipse is defined as:

$$\rho_m + \rho_s = 2a \quad (4.1.4)$$

or in terms of the interfocal distance and eccentricity as:

$$\rho_m + \rho_s = \frac{2c}{e} \quad (4.1.5)$$

4.1.3.2 Reflection from the sub-reflector

The ellipse is rotated about its axis to form solid a figure that reflect incident spherical waves into spherical waves with different caustics (focus). The sub-reflector changes the curvature of waves coming from one focus into waves with their caustic at the second sub-reflector focus. In polar coordinates, this can be defined as:

$$\rho = \frac{eT}{1 - e\cos\theta} \quad (4.1.6)$$

where T is the distance from the focal point into a line called the *directrix* Figure 4.2(b) [47], ρ is the distance from the focus onto the sub-reflector surface and θ is the offset main reflector Figure 4.2(a).

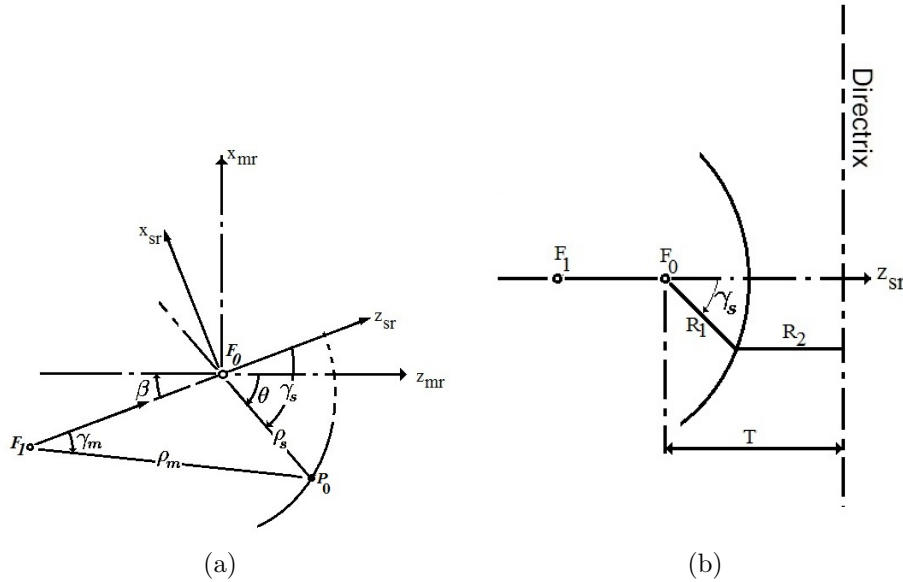


Figure 4.2: Ellipsoid geometry. (a) rectangular coordinate. (b) section of the ellipse sub-reflector

The eccentricity e of the sub-reflector is the ratio of the distance from the origin of a point on the curve to the distance from the same point to the directrix $e = \frac{R_1}{R_2}$. For a Gregorian system this distance T is given in terms of the interfocal distance as [16]:

$$T = \frac{c(1 - e^2)}{e^2} \quad (4.1.7)$$

Put (4.1.7) into (4.1.6), the distance from the left focus of the sub-reflector denoted ρ_m is:

$$\rho_m = \left(\frac{c}{e}\right) \frac{e^2 - 1}{e\cos\gamma_m - 1} \quad (4.1.8)$$

Chapter 4. Description of a Gregorian Reflector Antenna and Creation of a FEKO Reference

and the distance from F_0 onto the sub-reflector surface can be derived:

$$\rho_s = - \left(\frac{c}{e} \right) \frac{e^2 - 1}{e \cos \gamma_s + 1} \quad (4.1.9)$$

The projection of the line F_1P_0 onto the sub-reflector axis z_{sr} gives angle γ_m , and γ_s is the projection of the line F_0P_0 onto the z_{sr} axis. These angles are related by the eccentricity [48].

$$(e + 1) \tan \left(\frac{\gamma_m}{2} \right) = |e - 1| \tan \left(\frac{\gamma_s}{2} \right) \quad (4.1.10)$$

4.1.4 Equivalent parabola analysis

A dual offset reflector model can be geometrically transformed on its equivalent parabola. This new geometry is based on the optics theory and eases the analysis. This model geometry is illustrated in Figure 4.3. An equivalent parabola geometry has the same diameter as the dual offset ($D = D_{eq}$), but its focal length f_{eq} is longer than that of the paraboloid main reflector. The ratio of these 2 focal lengths is called the *magnification*, $M = f_{eq}/f$ for a Gregorian system, it is given in terms of the eccentricity by:

$$M = \frac{1 + e}{1 - e} \quad (4.1.11)$$

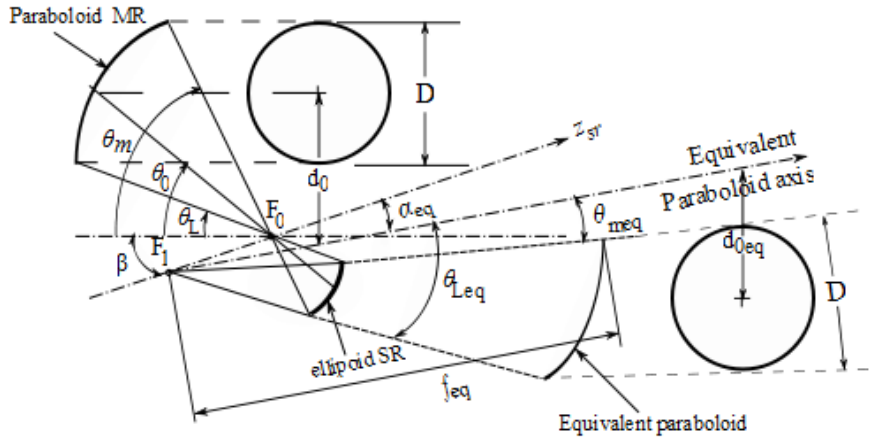


Figure 4.3: Equivalent paraboloid of a dual offset Gregorian geometry with circular aperture after [48]

The field of rays flowing from the source into a point on the aperture plane of the main reflector in the x-axis, if it has an equivalent paraboloid, is related as follows [48]:

$$E_P(\theta, \phi) = \frac{E(\theta, \phi)}{\rho_{eq}} \quad (4.1.12)$$

with

$$\rho_{eq} = \frac{2f_{eq}}{1 + \cos(\gamma_f)} \quad (4.1.13)$$

and the equivalent focal length is:

$$f_{eq} = f \frac{|e^2 - 1|}{(e^2 + 1) - 2e \cos \beta} \quad (4.1.14)$$

Equation(4.1.12) shows that the radiation aperture field at P is similar to that of the equivalent paraboloid. Then, the radiation aperture field of the equivalent paraboloid is similar to the aperture of an offset dual reflector antenna if the diffraction effects are ignored.

Based on the equivalent parabola principle, α is defined as the angle of orientation of the equivalent paraboloid. It depends on both the eccentricity of the ellipsoid sub-reflector and the angle β as indicated in (4.1.16). This is applied from the Muzigutchi condition, which is used to reduce the cross-polarization of the antenna systems [49][50].

$$\tan\left(\frac{\alpha}{2}\right) = \frac{|e^2 - 1|}{e^2 + 1} \tan\left(\frac{\beta}{2}\right) \quad (4.1.15)$$

or

$$\alpha = 2 \arctan \left[\frac{|e^2 - 1|}{e^2 + 1} \tan\left(\frac{\beta}{2}\right) \right] \quad (4.1.16)$$

The intersection of an ellipsoid with any circular cone having a vertex at either focus is a symmetric planar curve [51]. The equivalent paraboloid can be symmetric depending upon the selection of the antenna system parameters, which reduces the spillover losses.

Hence the offset dual reflector system with focused feed equivalent can be analysed as a single paraboloid surface.

4.1.5 Antenna design parameters

For this present case, five of these parameters described in Table 4.1 are defined as input parameters. D , θ_L for the prime reflector; β , L_{sr} for the sub-reflector and the ratio f/D . This last one is a free parameter for the engineer, which is in fact constrained in practice. A lower value of this parameter will bring the feed into the optical path, while too high value will place the feed behind the main reflector. Computation of the derived parameters obviously relies on the input. The design procedure will be started with a few steps of calculation.

4.1.5.1 Ellipsoid parameters

First, the eccentricity e of the sub-reflector depends strictly on the value of the angle β , which should be positive to avoid not only a complex value for e , but also a feed blockage

Chapter 4. Description of a Gregorian Reflector Antenna and Creation of a FEKO Reference

on the prime reflector. For the case of a Gregorian system, eccentricity is given by [46]:

$$e = \frac{1 - \sqrt{\frac{\tan(\beta/2)}{\tan(\beta-\theta)/2}}}{1 + \sqrt{\frac{\tan(\beta/2)}{\tan(\beta-\theta)/2}}} \quad (4.1.17)$$

V_s is the sub-reflector projection height, which is equal to the difference between the maximum and minimum values of the ellipse in x coordinate (x value of the points P_1 and P_2 respectively (see Figure 4.1).

$$V_s = x_{P_1} - x_{P_2} \quad (4.1.18)$$

from (4.1.9), the sub-reflector surface on the x_{sr} coordinate is derived

$$x_{sr} = \rho_s \sin\theta = -\left(\frac{c}{e}\right) \frac{(e^2 - 1)\sin\theta}{e\cos(\theta - \beta) + 1} \quad (4.1.19)$$

According to (4.1.19), the maximum and the minimum distance of the sub-reflector, which is related to x_{P_1} and x_{P_2} depends on the offset angle of the main reflector. Thus, the sub-reflector projection height can be expressed as:

$$V_s = \left(\frac{c}{e}\right) \frac{(e^2 - 1)\sin\theta_m}{e\cos(\theta_m - \beta) + 1} - \left(\frac{c}{e}\right) \frac{(e^2 - 1)\sin\theta_L}{e\cos(\theta_L - \beta) + 1} \quad (4.1.20)$$

and hence the interfocal distance of the ellipse can be taken from (4.1.20), and the minimum radius R_{min} of curvature of the sub-reflector can be calculated in terms of the eccentricity and interfocal distance (4.1.22).

$$c = \frac{eV_s}{(e^2 - 1) \left[\frac{\sin\theta_L}{e\cos(\theta_L - \beta) + 1} - \frac{\sin\theta_m}{e\cos(\theta_m - \beta) + 1} \right]} \quad (4.1.21)$$

$$R_{min} = \frac{c|e^2 - 1|}{e} \quad (4.1.22)$$

Angle α , defined as the feed angle, can be derived from the Muzigutchi condition in (4.1.16).

$$\alpha = 2\arctan \left[\frac{e + 1}{e - 1} \tan \left(\frac{\beta}{2} \right) \right] \quad (4.1.23)$$

The half subtended angle of the ellipse sub-reflector as viewed from the first focal point θ_e is computed from (4.1.10). From Figure 4.2, if the angle situated at the first focal point is expressed in terms of α and the angle on the second focal point represented by β , then angles can be expressed as: $\gamma_m = \alpha + \theta_e$ and $\gamma_s = \theta_L + \beta$. Thereafter (4.1.10) becomes:

$$\tan \left(\frac{\alpha + \theta_e}{2} \right) = \frac{1 - e}{1 + e} \tan \left(\frac{\theta_L + \beta}{2} \right) \quad (4.1.24)$$

and,

$$\theta_e = 2\arctan \left[\left(\frac{1-e}{1+e} \right) \tan \left(\frac{\theta_L - \beta}{2} \right) \right] - \alpha \quad (4.1.25)$$

4.1.5.2 Paraboloid design parameters

The main reflector is characterized by the distance d_c , which is equal to the difference between its lower rim and the upper rim of the sub-reflector in the x coordinate. It is convenient for this height to be positive, to eliminate blockage.

$$d_c = x_{Q1} - x_{P2} = d_0 - \frac{D}{2} + \left(\frac{c}{e} \right) \frac{(e^2 - 1)\sin\theta_L}{e\cos(\theta_L - \beta) + 1} \quad (4.1.26)$$

Let L_{mr} and L_{sr} be the length of the main and the sub-reflector on the z -axis, respectively. The maximum length of the system L_t is the sum of these two lengths. From Figure 4.1, these distances are $L_{mr} = \rho_m \cos\theta$ and $L_s = -\rho_{sr} \cos\theta$. Replacing ρ_m and ρ_s on each value respectively, then the maximum length of the system is given by:

$$L_t = L_{mr} + L_{sr} = \frac{2f\cos\theta_L}{1 + \cos\theta_L} + \left(\frac{c}{e} \right) \left(\frac{2\cos\theta_L(e^2 - 1)}{e\cos(\theta_L - \beta) + 1} \right) \quad (4.1.27)$$

From these design equations, values of the parameter are computed for $f/D = 0.33$ at a frequency $\text{Freq} = 1.25$ GHz, as illustrated in Table 4.2. Angles are in degrees and lengths or diameter are expressed in terms of the wavelength λ .

Table 4.2: Parameter Values computed from the design equations

Parameter	Value
D	50λ
d_0	25λ
β	33.28°
θ_L	0°
L_{sr}	16.67λ
α	-64.89°
e	0.36
c	3.71λ
d_c	0
L_t	23.55λ
θ_e	48.89°
R_{min}	8.95λ

The lower offset angle of the main reflector is equal to zero ($\theta_L = 0$). Thus, the system is situated on the main reflector z axis ($d_c = 0$). A 2D plot of the Gregorian model is depicted in Figure 4.4. Thereafter, parameter values are transferred in FEKO to create the corresponding 3D geometry.

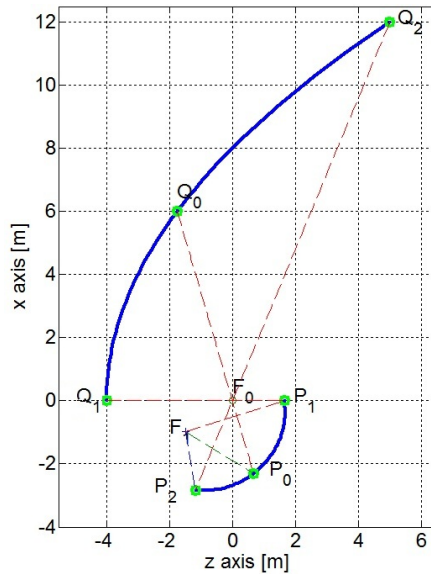


Figure 4.4: An offset Gregorian dual reflector antenna geometry generated in Matlab

4.2 Creation of a Gregorian antenna Reference in FEKO

4.2.1 The system feed

Selection of the feed system is one of the most important parts of the design. System requirements determine the feed type, which depends upon the frequency range of the antenna. A linear polarized application frequently uses a horn as a feed. This generally provides the most efficient antenna system for dual-reflector antennas and has very low insertion loss and often a Gaussian shape pattern that has minimal spillover loss [30]. The performance of antenna systems is improved by knowing the feed configurations. Horn or waveguide feeds with single mode are the most often used for antenna reflectors [28]. The ideal feed source with a radiation pattern as defined in (2.3.2) in §2.3, illuminates the sub-reflector.

4.2.1.1 Simulation in FEKO

An analytical function, which approximates the feed pattern, is generated in FEKO.

FEKO is a numerical electromagnetic software package. It is used for designing and investigating electromagnetic problems, based on a full wave solution of Maxwell's equations. FEKO uses Method of Moments (MoM) technique or hybrid methods including Physical Optics (PO), GO and GTD alongside with MoM for the analysis of electromagnetic problems. This technique is based on the integral equation and gives a solution in frequency domain.

Parameters in Table 4.2 were used to create the model of the dish reflector in FEKO. The source, linearly polarized, is positioned on the focal point of the reflector. The full Method

Chapter 4. Description of a Gregorian Reflector Antenna and Creation of a FEKO Reference

of Moments technique is used for various values of f/D to compute the antenna gain in the far field. Figure 4.5 depicts the orientation of the ideal source towards a paraboloid reflector in rectangular coordinates.

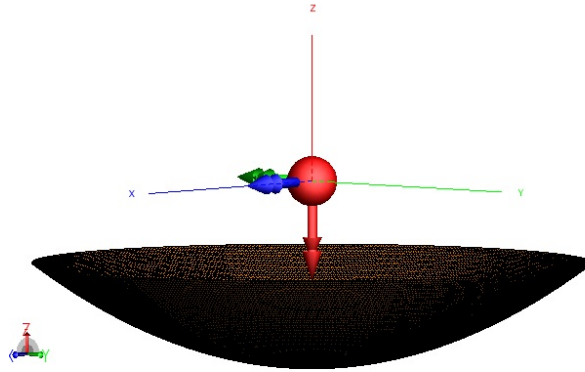


Figure 4.5: Ideal source oriented towards a paraboloid reflector with the diameter of the dish $D = 50\lambda$, generated with *FEKO*

4.2.1.2 Method Of Moments

Historically, Method of Moments technique or MoM was the first numerical method applied to electromagnetic problems in the 1960s [10]. Its principle is to transform an integro-differential equation into a set of simultaneous matrix equation (or linear equations) which may then be solved by numerical techniques.

With MoM technique, an equivalent current is computed to replace the scattering surface [52]. The conducting surfaces are segmented into small rectangles, which is called *meshing*. Then the normal surface currents are estimated on each rectangle by obtaining the current distribution on the surface. A fine mesh is required in MoM to obtain an accurate result. Using FEKO, a minimum mesh step size of one tenth of a wavelength is suggested [53].

4.2.1.3 Results gain of the feed

As mentioned earlier, for each variation of f/D there is only one maximum value of aperture efficiency each of the different feeds, which involves a maximum gain. The red curve represents the analytical approximation calculation and the plot in blue is the results from the CEM code in FEKO. Gain results are plotted in terms of the subtended angle θ_0 and compared in Matlab as illustrated in Figure 4.6.

Chapter 4. Description of a Gregorian Reflector Antenna and Creation of a FEKO Reference

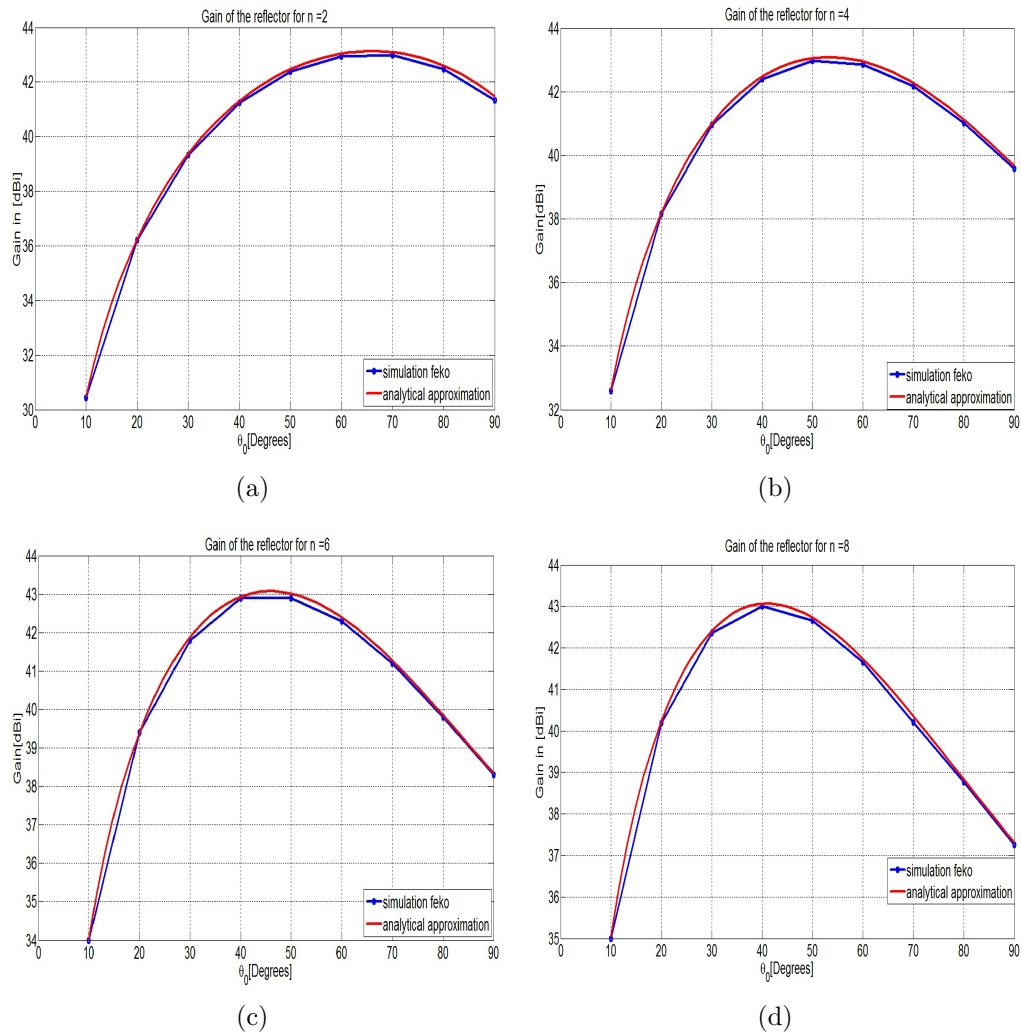


Figure 4.6: Comparison of approximate gain of the full-wave results from FEKO and the analytical approximation for different feed sources (a) $n=2$, (b) $n=4$, (c) $n=6$ and (d) $n=8$.

At high frequency, the diffraction effect on the dish edges can be neglected. Then, for a large electrical size of reflector, for example $D=50\lambda$ (reflector diameter), the full wave FEKO results and the analytical approximation agree well. The full-wave methods are accurate for the analysis of the reflector, but they are used especially for a small electrical size antenna because their computation run time tends to be intensive.

The analytical approximation run time is much faster than the MoM technique; a few seconds in Matlab against 5 minutes for numerical computation (FEKO) at a single frequency.

4.2.1.4 Advantages of using a dual reflector

The major advantage of using a dual offset reflector is that the feed does not block the aperture. Considering the equivalent parabola gives an easy analysis of the antenna reflector

Chapter 4. Description of a Gregorian Reflector Antenna and Creation of a FEKO Reference

characteristics. The axis of the equivalent paraboloid is oriented in the angular centre of the sub-reflector, this condition yielding an axially symmetric equivalent paraboloid, thereby minimizing spillover losses.

The ability to use computer-aided design (CAD) tools has become an essential requirement for a good antenna engineer. Furthermore, a large number of antenna design software packages and electromagnetic tools have been developed and have appeared on the market [10]. FEKO, which was used in this project, can even use hybrid methods to compute antenna properties. Besides this, the prime and sub-reflectors for a dual reflector model can be analysed by two different methods, for example to increase the speed of the simulation, or to make results more accurate.

4.2.2 Gregorian reflector antenna simulation using hybrid technique

The methods available to solve electromagnetic problems depend on the nature and size of the antenna. FEKO, which is a commercial electromagnetic package based on Method of Moment and extensions, is used to generate a reference solution of the antenna topology under consideration.

A 3D model of an offset Gregorian dual reflector antenna as generated by CADFEKO (a component of FEKO) as illustrated in Figure 4.7. The model is created using the variables listed in Table 4.3. The system axis defined by (x,y,z) , is placed at the dish focal point. The sub-reflector focal point F_0 . The distance $d_0 \geq 0$ is chosen to reduce the feed blockage by putting the sub-reflector on the boundary of the main beam. Radiation from the source is deflected by the ellipsoidal sub-reflector through its virtual focal point F_1 . This point is coincident with the focus on the dish main reflector; this main reflector will collimate the beam to give the pencil beam radiation pattern of the system.

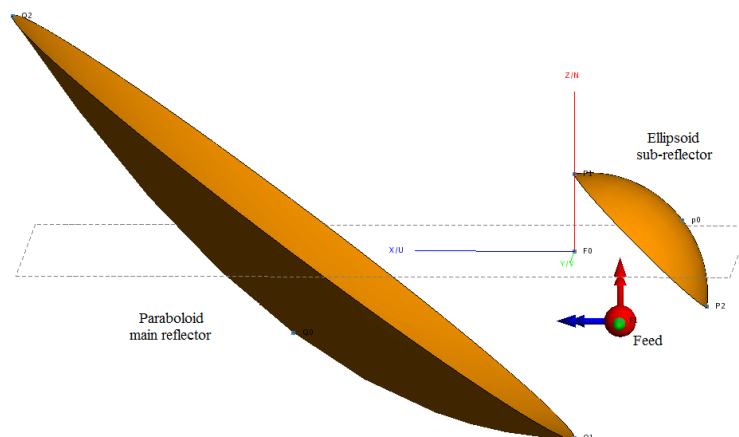


Figure 4.7: 3D Geometry of an Offset Gregorian Dual reflector generated from CADFEKO

Table 4.3: Parameters of the antenna design

	Parameter	Values	Unit
<i>Antenna system</i>	f/D	0.33	
	Lm	36.172	λ
	Lt	23.626	λ
	Ht	61.987	λ
<i>Main Reflector</i>	D	50	λ
	f	16.66	λ
	d_0	0	λ
	h	25	λ
	θ_0	-1.287	rad
	θ_m	-1.966	rad
<i>Sub-Reflector</i>	c	3.708	λ
	V_s	11.82	λ
	R_{min}	8.984	λ
	L_{sr}	16.67	λ
	L_s	10.606	λ
	β	0.581	rad
	θ_e	0.853	rad
	α	-1.133	rad
	e	0.360	

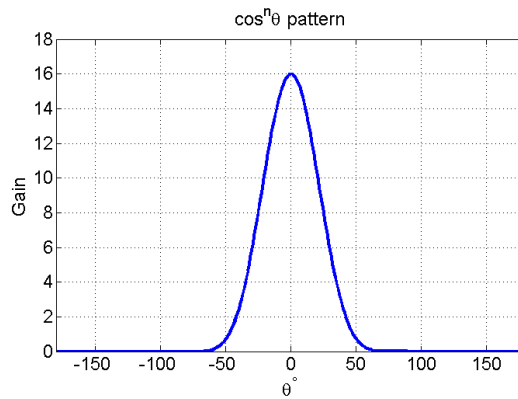
4.2.2.1 FEKO simulation set-up

The surface of the parabolic main reflector is large compared to the size of the sub-reflector, as shown in Table 4.3. The solution of such a problem can be better found by separating the solution in three steps as:

- Description of the feed pattern,
- Computation of the sub-reflector radiation pattern using the MLFMM technique in FEKO,
- Computation of the main reflector pattern using PO approximation.

4.2.2.2 Feed pattern description

The feed is simplified by recognising that a horns radiation pattern can be well approximated by an analytical formula which specifies the pattern as having a $\cos^n\theta$ dependence on the angle of boresight. This analytical function is generated by FEKO and its radiation pattern is shown in Figure 4.8.

Figure 4.8: Radiation pattern of the idealised feed $\cos^7\theta$.

4.2.2.3 Sub-reflector pattern

Figure 4.9 illustrates the 3D geometry of the ellipsoid sub-reflector generated by CAD-FEKO where the analytical feed pattern is used to excite the sub reflector. Adopting the FEKO guidelines, the sub-reflector is of moderate electrical size (up to approximately 10λ in diameter) and can be treated using the MoM formulation, and specifically the iterative MLFMM (Multi-level Fast Multipole Method) implementation thereof.

It is applied to accelerate the matrix-vector multiplication operation to solve the iteration of the matrix system. The MLFMM technique improves a slow solution time which is proportional to $N * [\log N]^2$ and requires a scaling in memory proportional to $O(N \log N)$, against $O(N^2)$ memory requirement and a computational complexity of $O(N^3)$ for MoM [53][54][55].

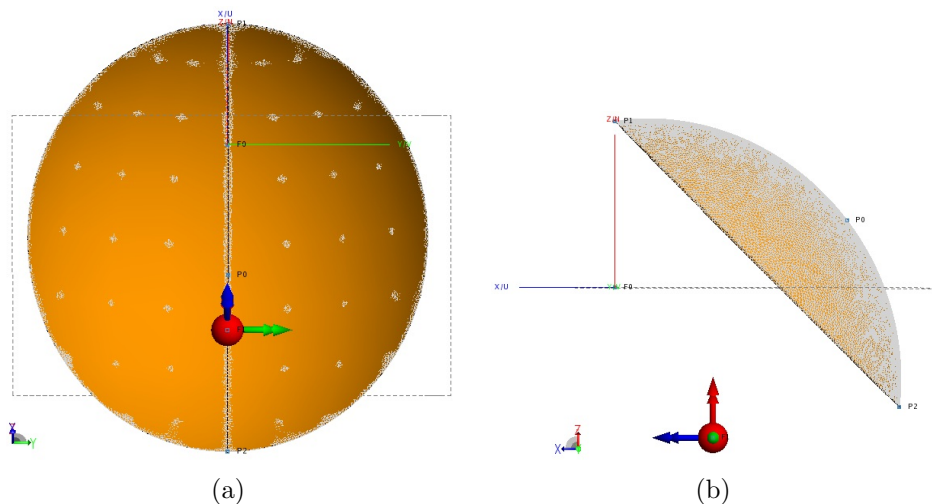


Figure 4.9: (a) Front and (b) side view of the ellipsoid sub-reflector oriented towards the feed source

Figure 4.10 shows the radiation pattern of the feed and sub-reflector combination. The

Chapter 4. Description of a Gregorian Reflector Antenna and Creation of a FEKO Reference

'ripple' in main beam is a result of the interaction of diffraction terms of the sub-reflector edges. This effect of amplitude of about ± 1 dB is significant because it is the first deviation from the GO solution to manifest as the model is run for descending frequencies.

Figure 4.10 shows that the amplitude of the ripple depends on the diffraction pattern of the sub-reflector. This diffraction pattern is frequency dependent.

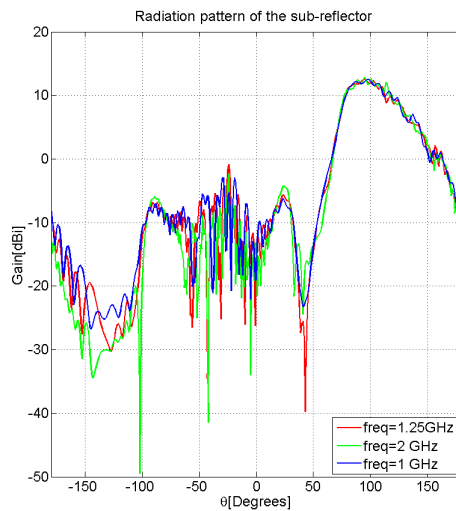


Figure 4.10: Radiation pattern of a 16.67λ sub-reflector illuminated with a -10 dB edge taper pattern at different frequencies.

4.2.2.4 Radiation pattern of the Gregorian antenna system

Once the feed and sub-reflector pattern is known this combined radiation pattern of the sub-reflector is saved in a FEKO ".ffe" file and is used to illuminate the main reflector. The new source is positioned at the focal point of the paraboloid main reflector, which is coincident with the virtual focal point of the sub-reflector. The limitation of this approach is that the dish should be in the far field of the sub-reflector and while this criterion is met at the upper frequencies.

The FEKO simulation provides an approximate full wave radiation pattern of the antenna system as shown in Figure 4.11.

Chapter 4. Description of a Gregorian Reflector Antenna and Creation of a FEKO Reference

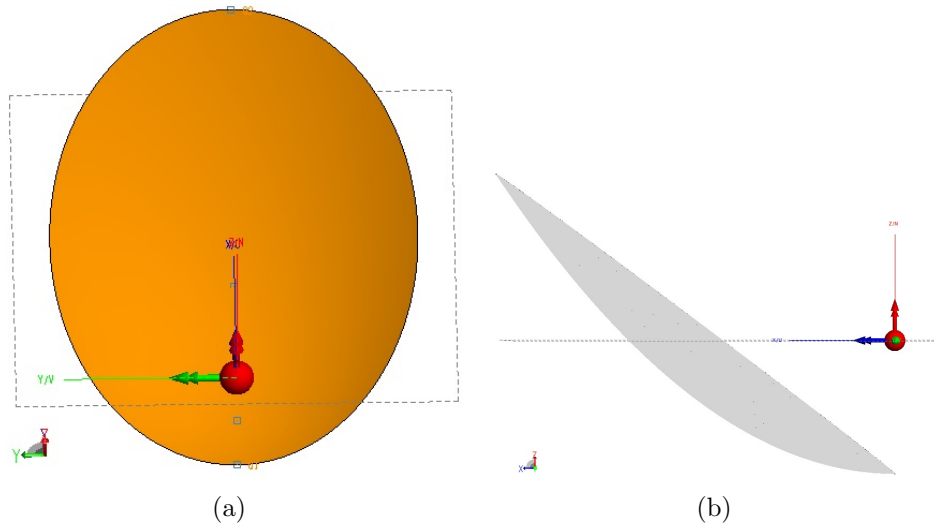


Figure 4.11: (a) front and (b) side view of the paraboloid main reflector pointed towards the new source with $D=50\lambda$, $\text{freq}=1.25\text{ GHz}$ and $f/D = 0.33$.

For a single frequency $\text{freq}=1.25\text{ GHz}$, the simulation for 6 hours for a full far-field solution (number of points 180×360) in FEKO by applying the hybrid method (PO + MLFMM). This simulation time is reduced somewhat by reducing a number of far field points but for a high gain antenna field points spaced a fraction of the beamwidth apart are required over the region of interest.

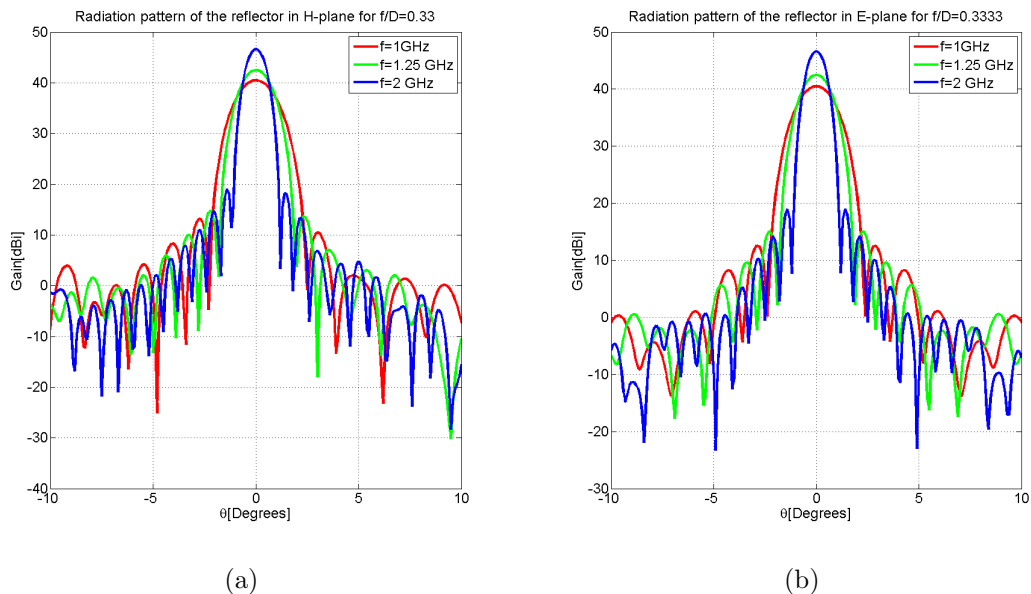


Figure 4.12: Radiation pattern of an offset Gregorian dual reflector antenna in (a): H- and (b): E-plane for different frequencies with $f/D=0.3333$.

Chapter 4. Description of a Gregorian Reflector Antenna and Creation of a FEKO Reference

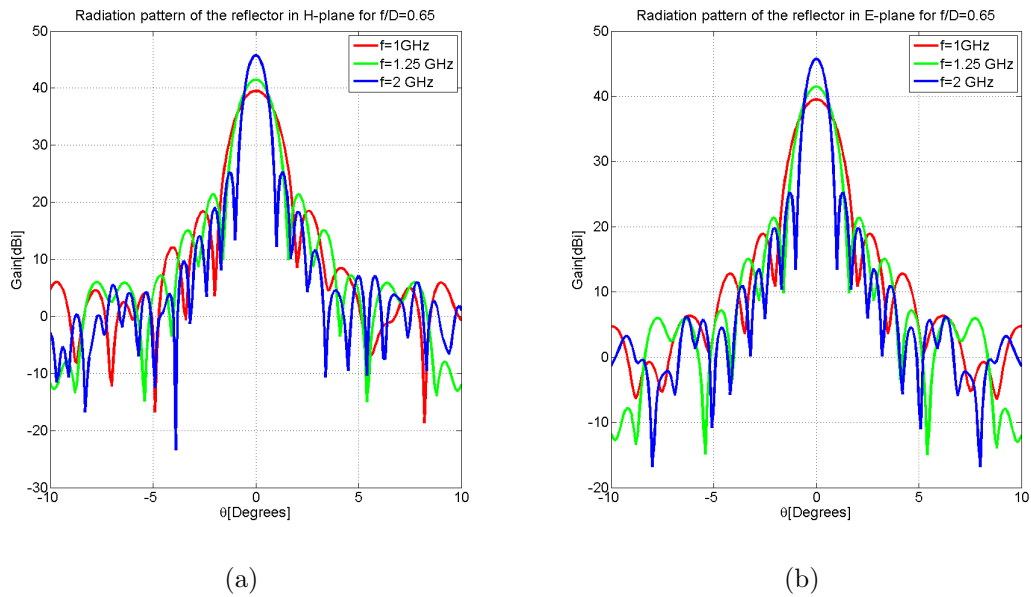


Figure 4.13: Radiation pattern of an offset Gregorian dual reflector antenna in (a): H- and (b): E-plane for different frequencies with $f/D=0.65$.

Results in Figure 4.12 illustrate the frequency dependence of the antenna gain and they show the advantages of using a reflector antenna, such as a high gain, narrow beamwidth and low side lobe level. By comparing Figure 4.12 and Figure 4.13, it is clear that the f/D parameter affects not only the gain but also the side lobe level, which increases with this parameter.

4.3 Conclusion

The classical design of a dual offset Gregorian reflector antenna requires an analysis of several parameters of the feed or reflectors. However, some of them can have a trade-off depending upon the application. Maximum gain is obtained when the feed is pointed at the focal point of the sub-reflector, while displacement of the source towards the sub-reflector can reduce the diffraction effects. Furthermore, the high frequency technique is suitable for the analysis of a dual reflector antenna. The computation effort is however too large for the fast iterative analysis, an approximate solution is then proposed as a fast and practical way of investigating the reflector pattern.

Chapter 5

Fast Approximation Technique for Reflector Antenna Patterns

Introduction

DETERMINATION of the radiation pattern is the major issue in this antenna characterization. A fast approximate solution to the radiation pattern of a Gregorian antenna is discussed in this chapter. Three steps are involved:

- find an equivalent feed pattern including an approximate diffraction term. To do this:
 1. The feed pattern is approximated by an analytical function, as was done for the FEKO model.
 2. The E-field that the feed generates at the sub-reflector is found using the Plane Wave Spectrum (PWS) of the feed. To do this:
 - (a) the analytical radiation pattern is converted to a Plane Wave Spectrum, which requires only the introduction of a cos term;
 - (b) As the axis of the feed horn is not perpendicular to the aperture of the sub-reflector an axis rotation of the field is required. In accordance with Fourier theory this is accomplished by adding a linear phase delay term in the opposite domain, which in this case is the spatial domain.
 3. The focussing effect of the sub-reflector is now taken into account by adjusting the phase of the field. This is done by first finding the point of reflection for any ray and then the required phase delay can then be found as the product of the wave number and the physical distance from the aperture plane to the reflection point and back.

4. The limited size of the sub-reflector can now be taken into account by truncating the field outside of the reflector region. This introduces an approximate diffraction effect.
 5. Transforming the field back to the source produces the equivalent feed pattern inclusive of an approximate diffraction term.
- the offset dual reflector geometry is replaced with an equivalent parabola,
 - find the radiation pattern of the equivalent system by combining the standard aperture integration technique with the Gauss- Legendre quadrature integration technique [19].

5.1 Radiation pattern of the sub-reflector using PWS

In this quasi-analytical approximation approach, an equivalent parabola geometry is considered; the two reflectors are pointed towards the feed source, wherein only the feed axis is considered for the entire problem.

The feed located at the second focal point of the ellipse forms a beam parallel to the focal axis and its pattern intensity is approximated from an analytical function given by (2.3.2). The radiation properties in the sub-reflector focal region are found by computing the plane wave spectrum integral using FFT algorithm.

A rectangular mesh grid is created at the feed axis, the size of the aperture is taken to be equal to the size of the sub-reflector, as illustrated in Figure 5.1(b). The mesh grid is created by the following expressions[56][6]:

$$\Delta x = \frac{L_{sr}}{Nx - 1}, \quad x = -\frac{L_{sr}}{2} + m\Delta x, \quad -\frac{Nx}{2} \leq m \leq \frac{Nx}{2} - 1 \quad (5.1.1a)$$

$$\Delta y = \frac{L_{sr}}{Ny - 1}, \quad y = -\frac{L_{sr}}{2} + n\Delta y, \quad -\frac{Ny}{2} \leq n \leq \frac{Ny}{2} - 1 \quad (5.1.1b)$$

where Nx and Ny are the number of points distributed in the x-and y direction of the aperture plane respectively. Δx and Δy represent the sample spacings. The selection of Δx and Δy will lead to PWS equally spaced in k-space. The sample spacings and spectral extents are given as:

$$\Delta x = \frac{\pi}{k_{x0}} \quad (5.1.2a)$$

$$\Delta y = \frac{\pi}{k_{y0}} \quad (5.1.2b)$$

where k_{x0} and k_{y0} , real numbers, denote the largest magnitudes of kx and ky respectively.

The corresponding spectral spacings Δkx , Δky in k space are given respectively by:

$$\Delta kx = \frac{2\pi}{Nx\Delta x} \quad (5.1.3a)$$

$$\Delta ky = \frac{2\pi}{Ny\Delta y} \quad (5.1.3b)$$

The spacing between the sampling points should be less than or equal to $\lambda/2$ to satisfy the Nyquist criterion. Reduction of this sampling interval has no benefit for a higher resolution in the far field.

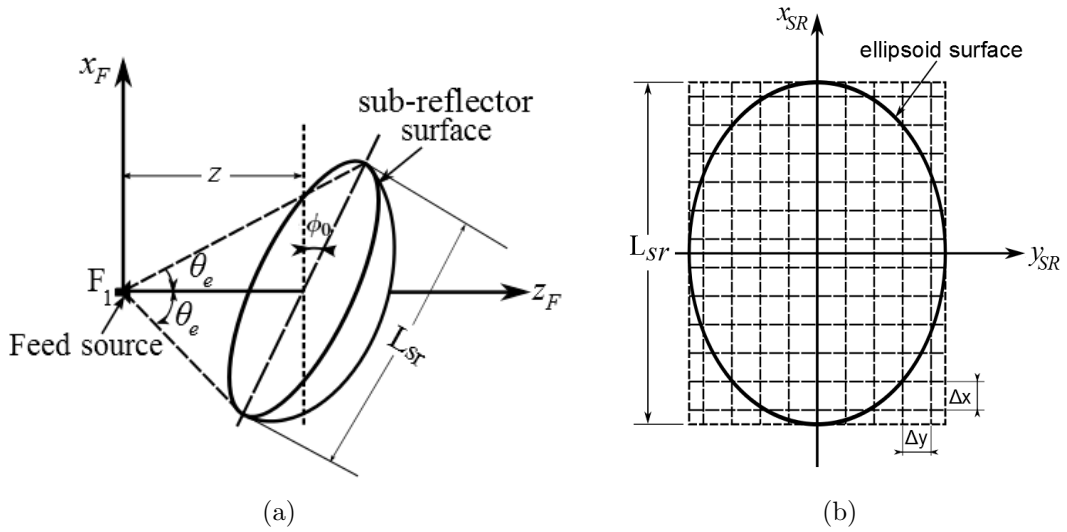


Figure 5.1: (a): Projection of the sub-reflector towards the feed axis, z : distance from the source to the sub-reflector aperture. (b): rectangular mesh grid for the sub-reflector view from the top of its axis. L_{sr} is the maximum aperture of the sub-reflector. [56]

Assume that the offset Gregorian dual reflector antenna has a secondary geometric optics focus at the location of the phase centre of the feed source. Only one reflected ray can be drawn from the source through the sub-reflector to each point on the main reflector surface, and the reflected ray to each point on the main reflector rim corresponds to a reflection point on the sub-reflector rim [57].

The sub-reflector is tilted at an angle ϕ_0 in the feed z -axis, as is shown in Figure 5.1(a). The radiated field from the sub-reflector will have a sharp cutoff at the shadow boundary; for a large diameter sub-reflector, the scattered field observed appears to have a sharp discontinuity.

The sub-reflector aperture field is evaluated from the feed pattern using the geometrical optics method. Assuming that this feed pattern is uniform, then only the propagator factor term, e^{-jkz} , is rotated on the y -axis, instead of rotating the feed pattern. Figure 5.2 shows the sub-reflector with the rotated E-field on the aperture plane, sampled with $\Delta x = \Delta y = \lambda/2$

Chapter 5. Fast Approximation Technique for Reflector Antenna Patterns

and $Nx = Ny = 512$. The correct E-field over the sub-reflector surface is obtained by adding a phase term on this rotated aperture E-field.

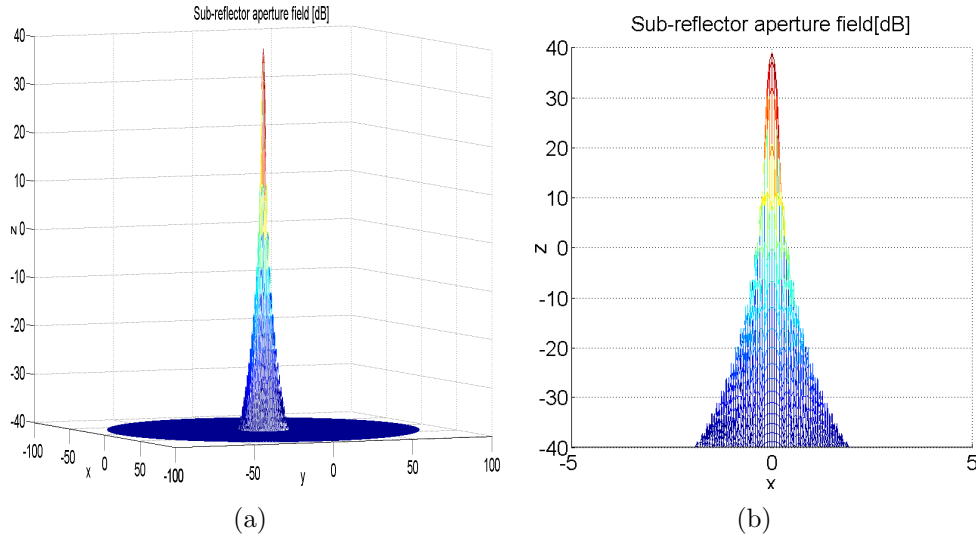


Figure 5.2: (a) 3D and (b) front view of the E-field on the sub-reflector rotation as a function of ϕ_0 .

The field on the sub-reflector aperture is cut-off (see Figure 5.3); the difference between the aperture field into this truncation will give the diffracted term on the sub-reflector as shown in Figure 5.4.

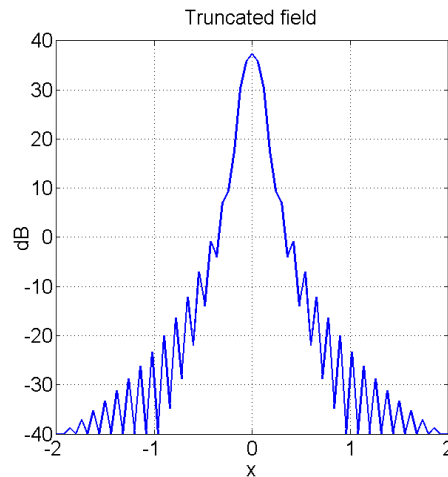


Figure 5.3: Truncated sub-reflector aperture field

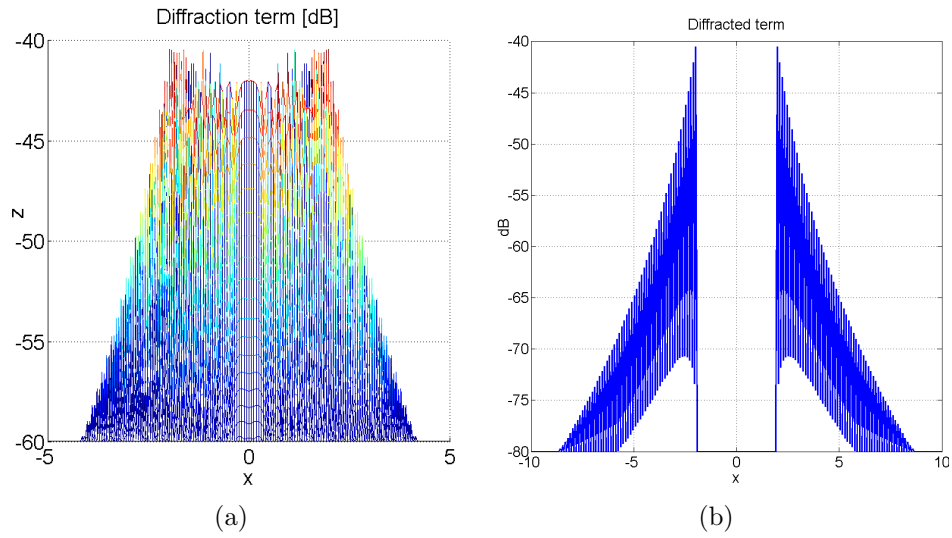


Figure 5.4: (a): 3D and (b): 2D view of the diffraction term on the sub-reflector

The diffraction approximation is given by adding this $\cos^n\theta$ with the back transformation of the diffraction term of the sub-reflector aperture at the origin (see Figure 5.5). The back transform pattern is obtained from the two-dimension iFFT algorithm. So the approximate diffraction pattern U_{feed}^d can be defined in term of the diffraction term D_{term} as:

$$U_{feed}^d = U_{feed} + D_{term} \quad (5.1.4)$$

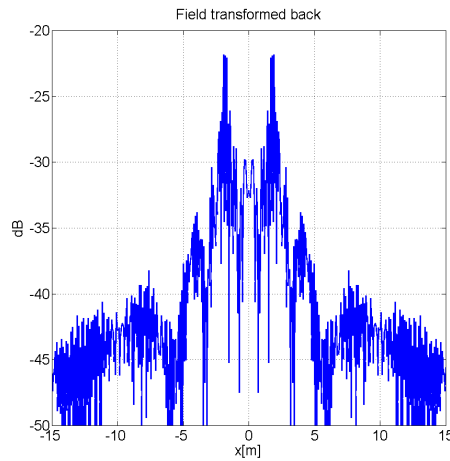


Figure 5.5: Diffraction term back transformed at the origin

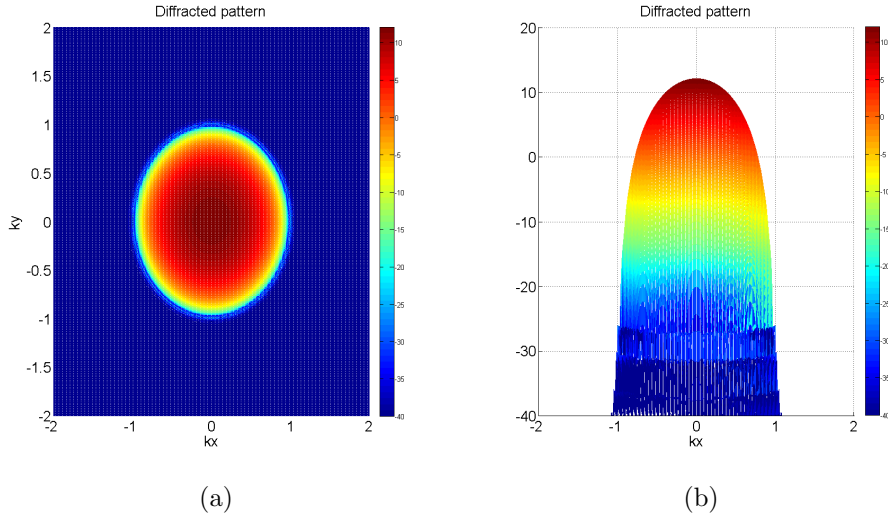


Figure 5.6: (a): Top and (b): side view of sub-reflector cut pattern

This diffracted pattern shown in Figure 5.6 is used as a new source for the evaluation of the radiation properties of the equivalent parabola.

5.2 Radiation of the main reflector

5.2.1 Aperture Integral Technique

The Aperture Integral technique is used to evaluate the main beam and near side lobes of the reflector antenna pattern. Assuming that U_{feed}^d is the approximate diffracted feed pattern. The aperture field of the reflector can be determined from the field radiated by the feed. The feed's radiation intensity U_{feed}^d is related to the aperture field as [19]:

$$U_{feed}^d = R^2 \frac{1}{2\eta} |E_i|^2 = \frac{1}{2\eta} |f_i(\theta', \phi')|^2 \quad (5.2.1)$$

Assuming that the reflector is perfectly conducting, then the reflected field must satisfy the relationship $\hat{n} \cdot E_r = \hat{n} \cdot E_i$, which implies that fields have the magnitude ($|E_r| = |E_i|$). Next, the aperture field is obtained from the propagation of the radiated field E_r by a distance to the aperture:

$$E_a = \frac{e^{-2jkz_0}}{E_r} = \frac{e^{-jk(R+z_0)}}{R} f_r(\theta', \phi') \quad (5.2.2)$$

or this expression can be written in the parabola case as:

$$E_a = \frac{e^{-2jkF}}{R} f_a(\theta', \phi') \quad (5.2.3)$$

where θ' , ϕ' are the feed angles, and $F = R + z_0$ as depicted in Figure 5.7. f_a is the aperture pattern and $|f_a| = |f_r| = |f_i|$.

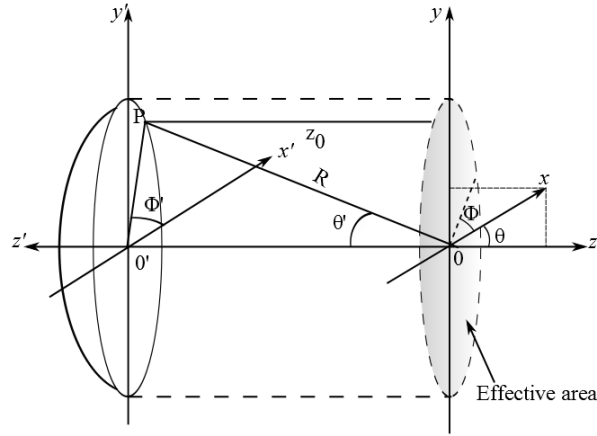


Figure 5.7: Parabolic main reflector pointed towards the diffracted source.

The radiation pattern of the main reflector can be evaluated from equations (3.5.10a) and (3.5.10b); where the vector $f = \hat{x}f_x + \hat{y}f_y$ is the Fourier transform over the reflector aperture:

$$f(\theta, \phi) = 2F e^{-2jkF} \int_0^{\theta'_0} \int_0^{2\pi} f_a(\theta', \phi') e^{2jkF \tan(\frac{\theta'}{2}) \sin\theta \cos(\phi - \phi')} \tan\frac{\theta'}{2} d\theta' d\phi' \quad (5.2.4)$$

in which F is the equivalent parabola focal length, θ'_0 is the reflector subtended angle. The 2D surface integral in (5.2.4) requires a computation time to get the radiation pattern of the antenna. However, because of the characteristics of the aperture field associated with the parabolic reflector, Gauss Legendre can be used to determine the radiation pattern.

5.2.2 Gauss Legendre technique

A Gauss-Legendre quadrature integration technique, which can be used to evaluate the numerical integral will approximate the integral into a double sum [19]:

$$f_A(\theta, \phi) = \sum_{i=1}^{N_1} \sum_{j=1}^1 w_{1i} F_A(\theta'_i, \phi'_j) w_{2j} = w_1^T F_A w_2 \quad (5.2.5)$$

where (w_{1i}, θ'_i) and (w_{2j}, ϕ'_j) are called *the quadrature weights* and computed over the intervals $[0, \theta'_0]$ and $[0, 2\pi]$; F_A is the matrix $F_A(\theta'_i, \phi'_j)$, and the two-dimensional Fourier

transform pattern is expressed by:

$$f_A(\theta, \phi) = \int_0^{\theta'_0} \int_0^{2\pi} F_A(\theta', \phi', \theta, \phi) d\theta' d\phi' \quad (5.2.6)$$

The H- and E-plane of the reflector radiation pattern is computed from (5.2.5) by setting $\phi = 0$ and $\pi/2$:

$$g_H(\theta) = |(1 + \cos\theta)f_A(\theta, 0)|^2 \quad H - plane \quad (5.2.7a)$$

$$g_E(\theta) = \left| (1 + \cos\theta)f_A\left(\theta, \frac{\pi}{2}\right) \right|^2 \quad E - plane \quad (5.2.7b)$$

Results below show the computation of the main beam and near side lobes using this method. The figures show that the beam width of the reflector is a frequency dependent and the side lobe level SLL varies with the edge illumination, i.e, augmentation of the f/D will increase the edge illumination.

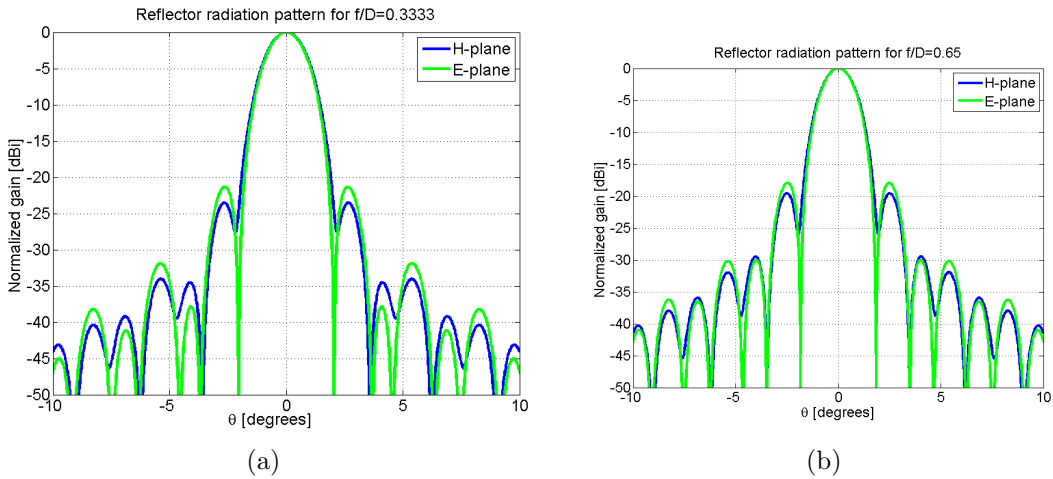


Figure 5.8: Offset Gregorian dual reflector radiation pattern for (a): $f/D=0.3333$, and (b): $f/D=0.65$ with $\text{freq}=1$ GHz.

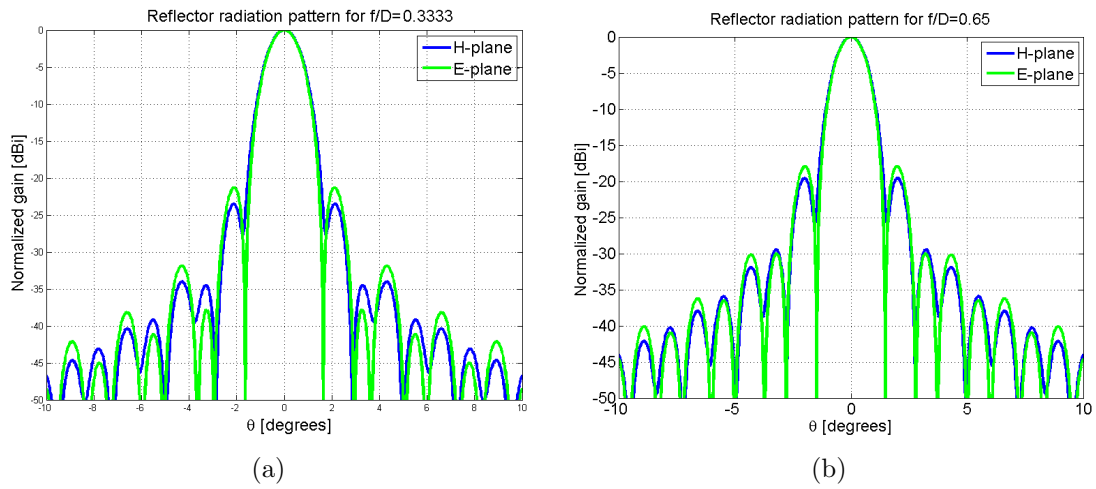


Figure 5.9: Offset Gregorian dual reflector radiation pattern for (a): $f/D=0.3333$, and (b): $f/D=0.65$ with $\text{freq}=1.25$ GHz.

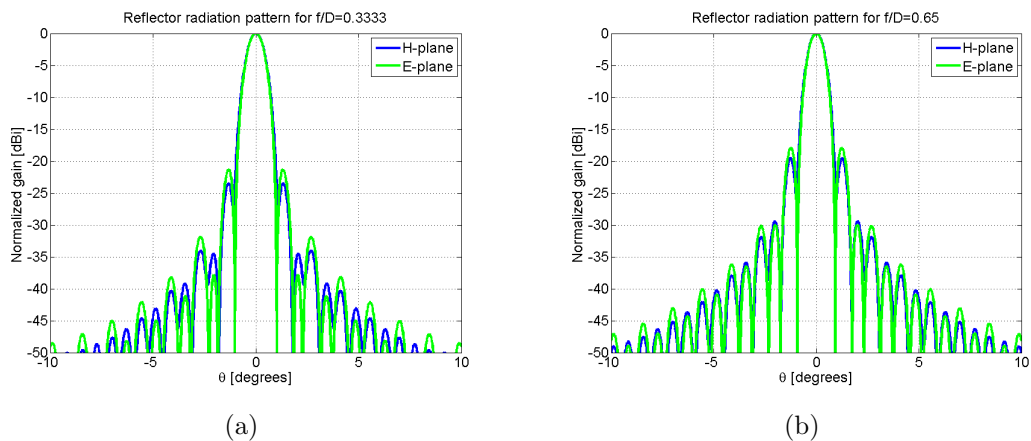


Figure 5.10: Offset Gregorian dual reflector radiation pattern for (a): $f/D=0.3333$, and (b): $f/D=0.65$ with $\text{freq}=2$ GHz.

5.3 Comparison of the fast approximation results with FEKO

Comparison is done for various frequency and f/D parameters.

Results from the numerical simulation in Figure 5.11-5.13 show that the beamwidth is originally wider than the analytical; which indicates that the simulation result is more tapered than the one for the fast approximation. The E and H-plane radiation pattern from the analytical approximation is symmetrical because of the use of the equivalent parabola geometry with a field polarized in \hat{y} direction. As mentioned earlier, the gain pattern of the dual reflector antenna depends on the frequency. For a lower frequency, 1 GHz for example,

Chapter 5. Fast Approximation Technique for Reflector Antenna Patterns

the numerical approach has 5 dB lower side lobe level than the fast approximation and this reduced at high frequency. These two methods have its advantages, however the fast approximation saves a time and reduces the memory requirement, by taking $N_x = N_y = 512$ sampling of points for the analytical computation.

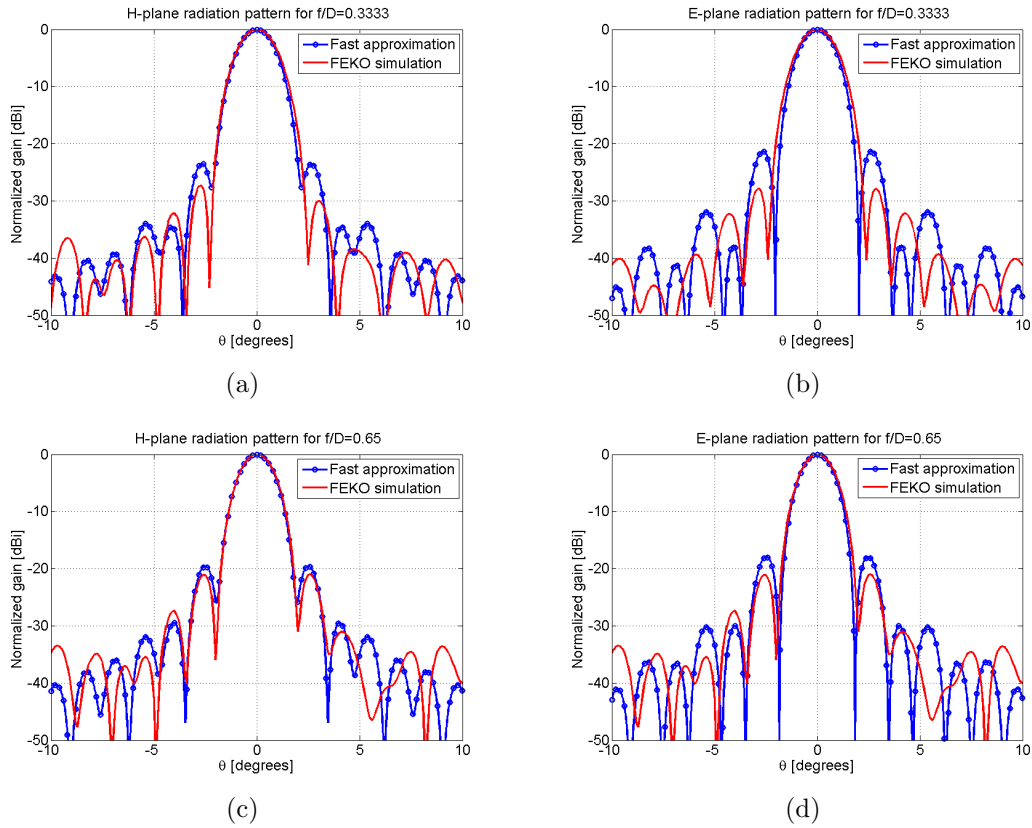


Figure 5.11: Comparison of the fast approximation technique and the numerical simulation of the dual reflector radiation pattern for $f/D=0.3333$ in (a): H-and, (b): E-plane, and for $f/D=0.65$ in (c): H-and, (d): E-plane at $\text{freq}=1$ GHz.

Chapter 5. Fast Approximation Technique for Reflector Antenna Patterns

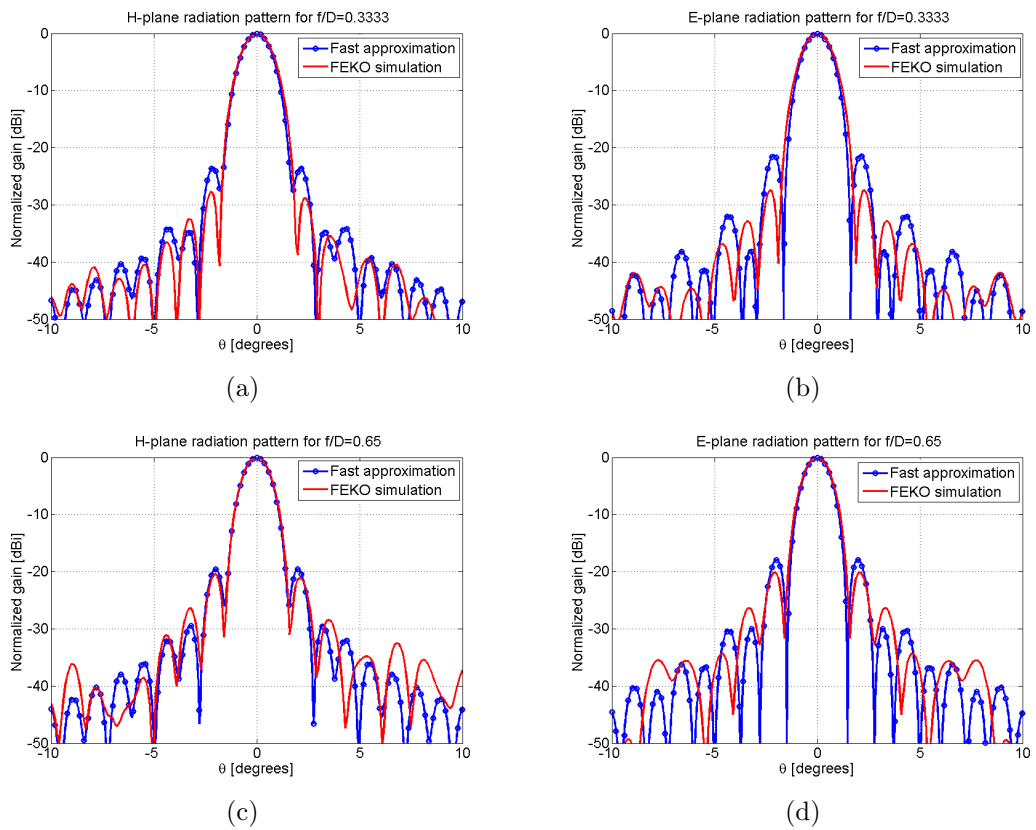


Figure 5.12: Comparison of the fast approximation technique and the numerical simulation of the dual reflector radiation pattern infor $f/D=0.3333$ in (a): H-and, (b): E-plane, and for $f/D=0.65$ in (c): H-and, (d): E-plane at $\text{freq}= 1.25$ GHz.

Chapter 5. Fast Approximation Technique for Reflector Antenna Patterns

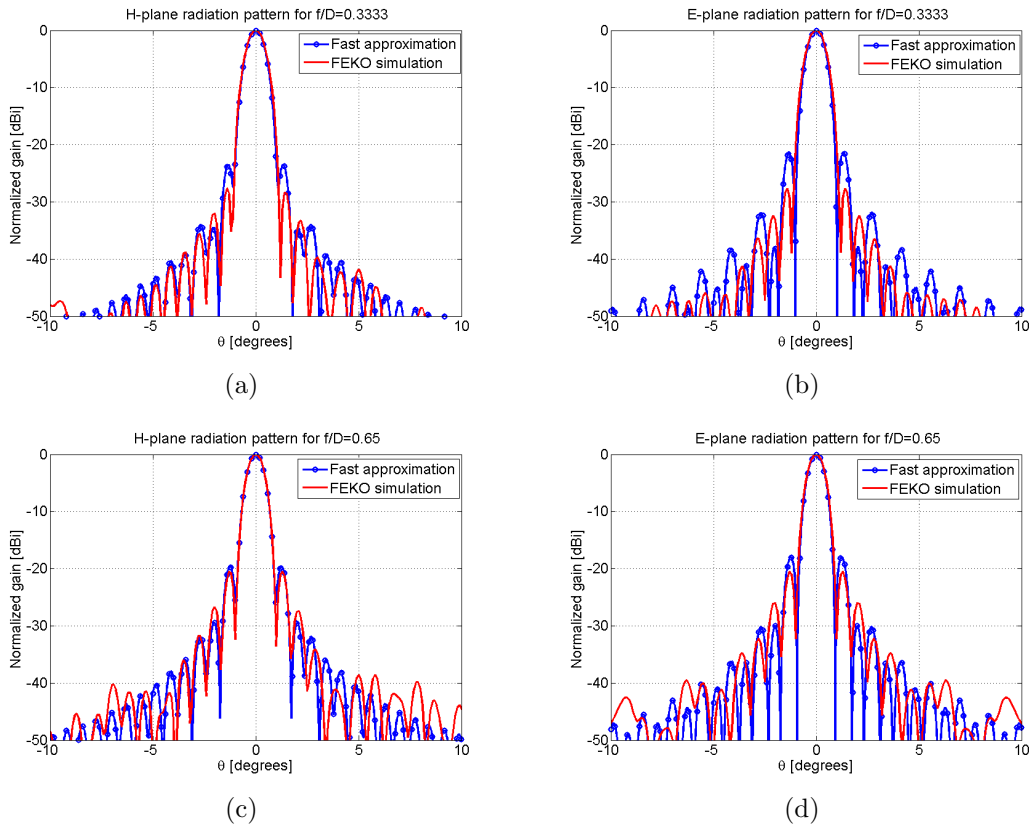


Figure 5.13: Comparison of the fast approximation technique and the numerical simulation of the dual reflector radiation pattern in for $f/D=0.3333$ in (a): H-and, (b):E-plane, and for $f/D=0.65$ in (c): H- and, (d): E-plane at freq= 2 GHz.

The fast approximation method is faster than the FEKO simulation. This analytical technique is accurate for the prediction of the main beam because of the application of the integral technique, however it cannot predict any information concerning the SLL, though it has less than 2 dB difference for a high edge illumination. In addition, the 3 dB beamwidth (HPBW) as listed in Table 5.1, enhances the performance of this fast approximation wherein the error is less at high frequency. For example, for a $f/D=0.3333$, at 1 GHz the beam width error is 8.18%, while it is reduced into 6.73% at 2 GHz in the E-plane.

Table 5.1: Comparison of the beamwidth results

f/D	Freq[GHz]	Type	FEKO[deg]	Fast appr.[deg]	Error[%]
0.3333	1	E-plane	0.8935	0.8204	8.18
		H-plane	0.8713	0.8456	2.95
	1.25	E-plane	0.7111	0.656	7.749
		H-plane	0.6978	0.679	2.70
	2	E-plane	0.4396	0.41	6.73
		H-plane	0.4333	0.4228	2.42
0.65	1	E-plane	0.8193	0.77	6.02
		H-plane	0.7911	0.794	0.367
	1.25	E-plane	0.6481	0.616	4.95
		H-plane	0.643	0.6448	0.28
	2	E-plane	0.4029	0.385	4.44
		H-plane	0.396	0.3969	0.23

The error in this table is given by the ratio of the difference between the FEKO and the fast approximation beam width to the beam width of FEKO as:

$$Error[\%] = \frac{|FEKO_{BW} - FastAppr_{BW}|}{FEKO_{BW}} \quad (5.3.1)$$

5.4 Matlab GUI application

This section will describe the implementation of a GUI generated in Matlab for a quick visualisation and investigation of the offset Gregorian dual reflector antenna geometry and its radiation pattern.

5.4.1 Overview of the GUI

A Graphical User Interface or GUI, is a figure window generated in Matlab, which has menus, text, graphics, etc., whereby the user can control interactively with the mouse and keyboard. In Matlab, a GUI design requires two principal steps: create the *layout* first, and write the *callback functions* that perform the desired operations [58].

The selection of the location and properties of the objects in a GUI can be achieved with certain commands such as, **uicontrol** and **uimenu** in the m-file. A tool called *GUIDE* provided by Matlab simplifies the access to handle graphics objects, and allows creation of GUI by clicking or moving the desired components off of a virtual menu.

By typing *guide* on the Matlab command window; the *Layout Editor* appears, which has a large white area with a grid. Layout editor contains a toolbar with short-cuts and provides

Chapter 5. Fast Approximation Technique for Reflector Antenna Patterns

a quick design of the interface. After saving this GUIDE, the m-file for the GUI will appear in a separate Editor/Debugger window. For each given object, a function callback can be created and edited in m-file.

5.4.2 GUI design

The GUI implemented in Figure 5.14 below consists of the following parts:

- the antenna input parameters,
- results of the computation for some parameters,
- plots of the geometry and the radiation pattern of the system.

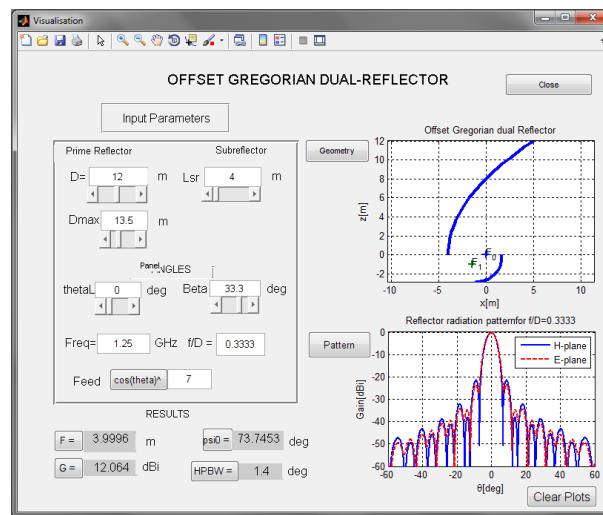


Figure 5.14: A quick visualisation of Gregorian dual reflector properties with a default parameters

5.4.2.1 Input parameters

The diameter D , the lower offset angle θ_L of the main reflector, the sub-reflector length L_{sr} and, the f/D of the system are defined as input parameters. Those parameters change the geometry of the antenna directly. Results which this GUI generates vary for a range of frequencies from 1 to 2 GHz.

5.4.2.2 Computation of results

For feeding reflectors, the program implements an ideal feed source given by $\cos^n\theta$ pattern. The radiation pattern of the antenna system is evaluated using the plane wave spectrum method. The sub-reflector pattern is evaluated from the spectrum based on the Fourier

transform, whereby the integral equation can be performed by the FFT algorithm. The Gauss Legendre technique is used to compute the integral equation of the main reflector pattern.

5.4.2.3 Plots of the Geometry and Pattern

The plot of the geometry, as well as the patterns and usual antenna parameters, are given in a well-organized manner on a single page, making it an easy task to compare the features of the various antenna geometries. The plot in Figure 5.14 shows the radiation pattern of the entire system in E- and H-plane, the geometry is plotted from the axis system, the gain of the feed and the 3-dB beam width of the equivalent parabola system.

The creation of this GUI will give the users a quick view of how the changing of the diameter of the reflector affects the gain. Equivalent parabola concepts are applied to investigate the gain and radiation pattern of the dual reflector antenna.

5.5 Conclusion

The fast approximation for the evaluation of reflector radiation pattern has been discussed in this chapter. As expected from the formulation the main beam from fast approximation agree well with the full wave with an error of 6.02% (1 GHz) at low frequency and 0.23% at 2 GHz for an $f/D=0.65$. The side lobe levels are not well predicted because of the complex formulation. The creation of GUI in Matlab is presented to analyse how change the parameters affect the radiation characteristics.

Chapter 6

Conclusions

Application of two different methods for the investigation of reflector antenna pattern has been done. The antenna geometry is generated and the radiation pattern is computed using an hybrid method. The simulation was split into two parts for the two different reflectors (sub-reflector and main reflector) to get results of greater accuracy and a radiation pattern point source has been used for the entire simulation to save on computational time and memory storage.

The radiation properties of this antenna have also been evaluated from a fast approximation technique based on the plane wave spectrum. The offset geometry was transformed into its equivalent parabola for this approach. A phase term was added to compensate the non-planar reflector.

This approach shows that the radiation far-field of the antenna relates to the Fourier transform of the aperture field and the double integrals of Fourier transform was solved using the FFT algorithm.

These two approaches are applicable for the reflector antenna analysis. The numerical computation was done an hybrid method, the feed pattern is used as a point source and the sub-reflector pattern is computed using MLFMM. Thereafter this sub-reflector pattern is used as a point source also pointed at the main reflector focal point and PO is applied on the main reflector.

This method requires an excessive time and memory, while the PWS application is faster than the hybrid method used in simulation, however it cannot gives any precision for the side lobes. An interface GUI in Matlab was generated, to give a quick visualisation of the radiation properties of an offset Gregorian dual reflector antenna using a plane wave spectrum approach.

Bibliography

- [1] S. Gregson, J. McCormick, and C. Parini, *Principles of Planar Near-Field Antenna Measurements*. Michael Faraday House Six Hills Way, Stevenage Herts, SG1 2AY, United Kingdom: Institution of Engineering and Technology, 2007.
- [2] P. J. Hall, *The Square kilometre Array: An Engineering Perspective*. P.O. Box 17, 3300 AA Dordrecht, The Netherlands: Springer Science, 2005.
- [3] S. A. S. K. A. T. P. Office, “South africa’s meerkat a centre of international attention.” <http://www.ska.ac.za/download>, March 2011.
- [4] J. L. Jonas, “The karoo array telescope,” *Cosmology and Galaxy Formation and Astroparticle Physics on the pathway to the SKA*, April 2006.
- [5] D. M. Pozar, *Microwave and RF design of wireless systems*. New York. Toronto. Singapore: John Wiley & Sons, Inc., 2000.
- [6] C. A. Balanis, *Antenna Theory: Analysis and Design*. Hoboken, New Jersey: John Wiley & Sons, Inc., 3rd ed., 2005.
- [7] “Parabolic reflector basics.” www.radio-electronics.com.
- [8] G. A. Thiele and S. W. L., *Antenna Theory and Design*. John Wiley & Sons, Inc., 1981.
- [9] T. C. of IEEE Society, “Ieee standard definitions of terms for antennas,” March 1993.
- [10] Y. Huang and K. Boyle, *Antennas from Theory to Practice*. The Atrium, Southern Gate, Chichester, West Sussex, PO19 8SQ, United Kingdom: John Wiley & Sons Ltd., 2008.
- [11] P.-S. Kildal, “Factorization of the feed efficiency of paraboloids and cassegrain antennas,” *IEEE transactions on antennas and Propagat*, vol. 33, pp. 903–908, August 1985.
- [12] S. Silver and H. M. James, *Microwave Antenna Theory and Design*. New York, Toronto, London: Mc Graw Hill book company, INC., 1949.

Bibliography

- [13] <http://www.orbitfr.com>.
- [14] C. F. L. Lew, "Inverted trapezoidal antenna for pulsed application," Master's thesis, The University of Queensland School of Information Technology & Electrical Engineering, St Lucia, Queensland, 4072, 2003.
- [15] A. C. Ludwig, "Definition of cross polarization," *IEEE transactions on antennas and Propagat*, pp. 116–119, January 1973.
- [16] T. A. Milligan, *Modern Antenna Design*. Hoboken, New Jersey: John Wiley & Sons, PUBLICATION, 2nd edition ed., 2005.
- [17] J. D. Kraus and K. R. Carver, *Electromagnetics*. Mc Graw Hill book company, 2nd ed., 1981.
- [18] B. S. Guru and H. R. Hiziroglu, *Electromagnetic Field Theory Fundamentals*. The Edinburgh Building, Cambridge CB2 2RU, UK: Cambridge University Press, 2nd ed., 2004.
- [19] <http://www.ece.rutgers.edu/orfanidi/ewa/>.
- [20] J. Häkli, *Shaped Reflector Antenna Design and Antenna Measurements at Sub-mm Wavelengths*. PhD thesis, Helsinki University of Technology, August 2006.
- [21] S. AKHMANOV and S. Y. NIKITIN, *Physical Optics*. Oxford University press. Great Clarendon Street, Oxford ox2 6dp, 1997.
- [22] J. Häkli, T. Koskinen, J. Ala-Laurinaho, J. Saily, A. Lonnqvist, J. Mallat, J. Tuovinen, and A. V. Raisanen, "A dual reflector feed system of a sub-mm hologram catr," *13th international symposium on space Terahertz Technology Harvard University*, pp. 327–336, March 2002.
- [23] R. G. Kouyoumjian, "Asymptotic high frequency methods," *Proceeding IEEE*, vol. 53, pp. 864–876, August 1965.
- [24] C. A. Balanis, *Advanced Enginnering Electromagnetics*. John Wiley & Sons, Inc., 1989.
- [25] A. Karttunen, "Design of a 650 ghz dual reflector feed system," Master's thesis, Department of Electrical and Communications Engineering Helsinki University of Technplogy, May 2006.
- [26] S. Boonsalee, "Effect of random surface errors on the performance of a paraboloid reflectors," Master's thesis, Massachusetts Institute of Technology, February 2000.
- [27] M. I. Skolnik, *Radar Handbook*, vol. 3rd. The McGraw-Hill Companies., 2008.

Bibliography

- [28] Y. T. Lo and S. W. Lee, *Antenna Handbook Antenna Theory*, vol. 2. 115th Avenue New York, NY 10003: van Nostrand Reinhold, 1993.
- [29] W. A. Imbiale and R. E. Hodges, "Linear phase approximation in the triangle facet near-field physical optics computer program," *Appl. Computational Electromagn. Soc.*, vol. 6, no. 2, pp. 74–85, 1991.
- [30] C. A. Balanis, *Modern Antenna Handbook*. 111 River Street, Hoboken, NJ 07030: A John Wiley & Sons, Inc., Publication, 2008.
- [31] M. Born and E. Wolf, *Electromagnetic Theory of propagation, interference and diffraction of light*. The Edinburgh Building, Cambridge CB2 2RU, UK: Cambridge University Press, 7th ed., 1999.
- [32] Y. Z. UMUL and U. YALCIN, "Asymptotic evaluation of the edge diffraction in cylindric paraboloid reflector antennas," *Mathematical and Computational Applications*, vol. 8, no. 2, pp. 143–150, 2003.
- [33] J. B. Keller, "Geometrical theory of diffraction," *Journal of the Optical Society of America*, pp. 116–130, February 1962.
- [34] D. A. McNamara, C. I. Pistorius, and J. G. Malherbe, *Introduction to the Uniform Geometrical Theory of Diffraction*. 685 Canton Street Norwood, MA 02062: Artech House, August 1989.
- [35] T.-H. Lee, "Geometrical optical optics and geometrical theory of diffraction analysis of subreflectors in cassegrain and gregorian reflector antennaa," Master's thesis, the Ohio State Univerity, 1984.
- [36] P. Y. Ufimtsev, *Fundamentals of the Physical Theory of Diffraction*. Hoboken, New Jersey: JohnWiley & Sons, Inc., 2007.
- [37] G. Ahmad and S. A. Mohsin, "High frequency techniques for reflector antenna analysis," *Electrical Engineering ICEE '09. Third International Conference*, pp. 978–984, July 2009.
- [38] A. Michaeli, "Elimination of infinities in equivalent edge currents, part i: Fringe current components," *IEEE transactions on antennas and Propagat.*, vol. AP-34, no. 7, pp. 912–918, 1986.
- [39] C. E. RYAN, "Evaluation of edge-diffracted fields including equivalent currents for the caustic regions," *IEEE transactions on antennas and Propagat.*, vol. AP-17, no. 3, pp. 292–299, 1969.

Bibliography

- [40] J. P. McKay and Y. Rahmat-Samii, "Compact range reflector analysis using the plane wave spectrum approach with an adjustable sampling rate," *IEEE transactions on antennas and Propagat*, vol. 39, pp. 746–753, June 1991.
- [41] R. Clarke and J. Brown, *Diffraction Theory and Antennas*. Marker Cross House, Cooper Street, Chichester, West Sussex, PO19 1EB, England: Ellis Horwood Limited, 1980.
- [42] P. C. Clemmov, *The Plane Wave Spectrum Representation of Electromagnetic Fields*. 445 Hoes Lane, PO Box 1331 Plscatawaty NJ 08855-1331: IEEE press, 1966.
- [43] T. B. Hansen and A. D. Yaghjian, *Plane- wave theory of time-domain fields Near-Field Scanning Applications*. 445 Hoes Lane, PO. Box 1331 Piscataway, NJ 08855-1331: IEEE Press Series on Electromagnetic Wave Theory, 1999.
- [44] E. V. Jull, *Aperture Antennas and Diffraction theory*. Stevenage, UK and New York: The Institute of Electrical Enginners, London and New York, 1970.
- [45] T. Milligan, "Designing classical offset cassegrain or gregorian dual reflector antennas from combinations of prescribed geometric parameter," *IEEE transactions on antennas and Propagat Magazine*, vol. 44, pp. 114–123, June 2002.
- [46] K. W. Brown and A. P. Jr., "A design procedure for classical offset dual reflector antennas with circular apertures," *IEEE transactions on antennas and Propagat*, vol. 42, pp. 1145–1153, August 1994.
- [47] M. R. SPIEGEL, *Mathematical Handbook of Formulas and Tables*. Reading, MA: McGraw-Hill, 1968.
- [48] W. V. T. Rusch, L. P. Jr., Y. Rahmat-Samii, and R. A. Shore, "Derivation and application of the equivalent paraboloid for classical offset cassegrain and gregorian antennas," *IEEE transactions on antennas and Propagat*, vol. 38, pp. 1141–1149, August 1990.
- [49] S. Xu and Y. Rahmat-Samii, "A novel beam squint compensation technique for circularly polarized conic-section reflector antennas," *IEEE transactions on antennas and Propagat*, vol. 58, pp. 307–317, February 2010.
- [50] D. I. L. de Villiers, "Analytical prediction of feed efficiency in offset gregorian reflector antennas with non planar log-periodic type feeds," *PIERS online*, vol. 7, pp. 231–235, 2011.
- [51] V. Jamnejad-Dailami and Y. Rahmat-Samii, "Some important geometrical features of conic-section- generated offset reflector antennas," *IEEE transactions on antennas and Propagat*, vol. 28, pp. 952–957, November 1980.

Bibliography

- [52] D. B. Davidson, *Computational Electromagnetics for RF and Microwave Engineering*. The Edinburgh Building, Cambridge CB2 8RU, UK: Cambridge University press, 2005.
- [53] Feko, “Em software & systems-s.a. (pty) ltd.” <http://www.feko.info>.
- [54] A. Tzoulis and T. F. Eibert, “Combining the multilevel fast multipole method with the uniform geometrical theory of diffraction,” *Advances in Radio Science*, no. 3, pp. 183–188, 2005.
- [55] R. Chen, P. Rui, and Y. N. Gan, “Schwarz-krylov subspace method for mlfmm analysis of electromagnetic wave scattering problems,” *Progress in electromagnetics research*, vol. pier 82, pp. 51–63, 2008.
- [56] A. Z. Nezhad, Z. H. Firouzeh, and H. Mirmohammad-Sadeghi, “A fast method to compute radiation fields of shaped reflector antennas by fft,” *Advanced Microwave and Millimeter Wave Technologies: Semiconductor Devices and Circuits and Systems*, pp. 190–204.
- [57] P.-S. KILDAL, “The effects of subreflector diffraction on the aperture efficiency of a conventional cassegrain antenna- an analytical approach,” *IEEE transactions on antennas and Propagat*, vol. AP-31, no. 6, pp. 903–909, 1983.
- [58] R. Brian, H. Ronald, L. Lipsman, J. M. Rosenberg, K. R. Coombes, J. E. Osborn, and G. J. Stuck, *A Guide to MATLAB for Beginners and Experienced Users*. Cambridge University Press, 2001.

Appendices

Appendix A

Analytical evaluation of directivity using spectrum [1].

A.1 Directivity using PWS

The directivity of a reflector antenna can be compute from the feed pattern. It is defined as the ratio of the maximum radiation intensity of the antenna over the radiated power divided by unit of the solid angle.

$$D = 4\pi \frac{U_{max}}{P_{rad}} \quad (\text{A.1.1})$$

This radiation intensity is proportional to the far electric field as:

$$\underline{U}(\theta, \phi) = \frac{r^2}{2\eta} |\underline{E}(r, \theta, \phi)|^2 \quad (\text{A.1.2})$$

in which the far field, the electric field can be expressed as:

$$\underline{E}(r, \theta, \phi) = \frac{e^{-jkr}}{r} \underline{E}(\theta, \phi) \quad (\text{A.1.3})$$

where r is the radius and (θ, ϕ) is the angle in the far field. By replacing the electric field on each value given by (A.1.3). Then, (A.1.2) is reduced into:

$$\underline{U} = \frac{1}{2\eta} |\underline{E}(\theta, \phi)|^2 \quad (\text{A.1.4})$$

Appendix A. Analytical evaluation of directivity using spectrum [1].

The electric field also can be evaluated from the angular spectrum and it is expressed in rectangular coordinates as:

$$E(x, y, z) = \frac{1}{4\pi^2} \int_{-\infty}^{\infty} \int_{-\infty}^{\infty} F(kx, ky) e^{-j(kxx+kyy+kzz)} dkxdky \quad (\text{A.1.5})$$

where $F(kx, ky)$ describes the plane wave spectrum of the field; and (A.1.5) defines the relationship between the near-field zone and the far field for a planar systems.

A.2 The total radiated power

The time averaged power flux that is transmitted per unit area across an aperture plane, radiated by an arbitrary current density can be given by:

$$P_r = \frac{1}{2} \text{Re} \left\{ \int (\underline{E}_T \times \underline{H}_T^*) \cdot \hat{e}_z dx dy \right\} \quad (\text{A.2.1})$$

Taking the cross product of the tangential electric field and the complex conjugate of the tangential magnetic field yields.

$$(\underline{E}_T \times \underline{H}_T^*) \cdot \hat{e}_z = \begin{vmatrix} \hat{e}_x & \underline{E}_x & \underline{H}_x \\ \hat{e}_y & \underline{E}_y & \underline{H}_y \\ \hat{e}_z & 0 & 0 \end{vmatrix} \cdot \hat{e}_z = (E_x H_y^* - E_y H_x^*) \quad (\text{A.2.2})$$

Then (A.2.1) becomes:

$$P_r = \frac{1}{2} \text{Re} \left\{ \int E_x H_y^* dx dy \right\} - \frac{1}{2} \text{Re} \left\{ \int (E_y H_x^* dx dy) \right\} \quad (\text{A.2.3})$$

and from the Parseval's theorem [1], the total radiated power is given as:

$$P_r = \frac{1}{8\pi^2} \text{Re} \left\{ \int_{-\infty}^{\infty} \int_{-\infty}^{\infty} E_x H_y^* dkxdky \right\} - \frac{1}{8\pi^2} \text{Re} \left\{ \int_{-\infty}^{\infty} \int_{-\infty}^{\infty} E_y H_x^* dkxdky \right\} \quad (\text{A.2.4})$$